3-2021

# GPS-Denied Localization of Daughter-Ships in a Mother-Daughter Ship Collaborative Environment

Ethan W. Jacquin


# GPS-DENIED LOCALIZATION OF DAUGHTER-SHIPS IN A MOTHER-DAUGHTER SHIP COLLABORATIVE ENVIRONMENT

THESIS

Ethan W Jacquin, Captain, USAF

AFIT-ENG-MS-21-M-051

**DEPARTMENT OF THE AIR FORCE**
**AIR UNIVERSITY**

***AIR FORCE INSTITUTE OF TECHNOLOGY***

**Wright-Patterson Air Force Base, Ohio**

AFIT-ENG-MS-21-M-051

# GPS-DENIED LOCALIZATION OF DAUGHTER-SHIPS IN A MOTHER-DAUGHTER SHIP COLLABORATIVE ENVIRONMENT

THESIS

Presented to the Faculty

Department of Electrical and Computer Engineering

Graduate School of Engineering and Management

Air Force Institute of Technology

Air University

Air Education and Training Command

in Partial Fulfillment of the Requirements for the

Degree of Master of Science in Electrical Engineering

Ethan W Jacquin, B.S.E.E.

Captain, USAF

March 2021

AFIT-ENG-MS-21-M-051

# GPS-DENIED LOCALIZATION OF DAUGHTER-SHIPS IN A MOTHER-DAUGHTER SHIP COLLABORATIVE ENVIRONMENT

THESIS

Ethan W Jacquin, B.S.E.E.
Captain, USAF

Committee Membership:

Clark N Taylor, Ph.D
Chair

Scott L Nykl, Ph.D
Member

Robert C Leishman, Ph.D
Member

AFIT-ENG-MS-21-M-051

# Abstract

The Air Force and other Department of Defense (DoD) branches have expressed interest in small Unmanned Aerial Vehicles (UAVs) that can provide close-in sensing to a target of interest. These small UAVs can be launched from a "mothership" and can act autonomously to collect intelligence, overcome meteorological effects, or provide targeting solutions. However, the closer a UAV is to a target, the easier it will be to jam, spoof, or otherwise degrade Global Positioning System (GPS) signals. These signals are critical to the operation of the UAVs, or "daughter-ships", as the sensed data collected by the daughter-ships needs to be placed in a geodetic frame so that the mothership can take action on the collected data. Without accurate coordinates for the collected data, a daughter-ship's utility is dramatically reduced.

This research focuses on investigating the possibility of using the communication link between the mothership and daughter-ship as a replacement of GPS. Specifically, we are assuming a ranging link between the mothership and daughter-ship, and the mothership has not been denied GPS. Both the mothership and daughter ship are station keeping, but on significantly different orbits. A ranging link is used to measure the distance between the two ships at all times. Over the course of recording multiple different range measurements, a location for the daughter-ship can be estimated.

A simulation study was conducted to determine the viability of this approach. The simulation was designed using an Extended Kalman Filter (EKF) to analyze and predict the location of the daughter ship using only the range measurement between the two ships. Factors such as distance, altitude, roll angle, speed, ranging sensor noise, and inertial measurement unit (IMU) uncertainty were considered. The simulation confirmed that the approach was in fact viable and that error between the

truth data and predicted location can be generally kept below 3 meters.

Finally, a maximum error threshold of 3 meters was set in order to obtain the conditions at which this method would be viable. Parameters were set to a baseline value as described in this thesis, and single variables were altered to measure their effect on the ranging solution. From this, the magnitude of the errors were examined and a range of values in which the approach would yield acceptable results was formed.

The research closes by exploring additional options such as improving upon the simulation testing with real world hardware.

# Table of Contents

Page

# List of Figures

# List of Tables

GPS-DENIED LOCALIZATION OF DAUGHTER-SHIPS IN A
MOTHER-DAUGHTER SHIP COLLABORATIVE ENVIRONMENT

# I. Introduction

## 1.1 Problem Background

The Air Force and other Department of Defense (DoD) branches have expressed an interest in using small Unmanned Aerial Vehicles (UAVs) that can provide close-in sensing of a target of interest. These small, agile UAVs augment the versatile mission set of already existing platforms and can be launched from a "mothership" to be used in various roles including Intelligence, Surveillance, and Reconnaissance (ISR), to overcome weather or other meteorological effects, or even to provide targeting solutions. These platforms would likely be operated in hostile airspace where adversary action can jam, spoof, deny or otherwise degrade Global Positioning System (GPS) signals. These signals are critical to the operation of the UAVs, or "daughter-ships", as the mothership needs accurate positioning of the daughter-ship in order to take action upon the collected data. Without accurate positioning data, the usefulness of the daughter-ship data is severely reduced. Therefore, a solution is needed to allow the navigation of the daughter-ship in these hostile operational environments that is accurate enough to allow it to continue its mission relatively unimpeded. The solution should allow the daughter-ship to continue to pass useful information to the mothership so that it may act knowledgeably upon the data received. The proposed solution will achieve accurate localization of the daughter-ship by utilizing the ranging link between mothership and daughter-ship as a replacement of GPS.

## 1.2 Research Objectives

- Using a simulation environment, explore the viability of using the ranging link between the mother and daughter-ship to obtain a position solution of the daughter-ship.
- Determine the accuracy of the GPS-denied localization solution based on range measurements between the mother and daughter-ship.
- Examine the parameters which control the simulation and their effect on the accuracy of the position solution.
- Determine the range of parameters for which the localization solution will be effective.

## 1.3 Research Approach

Experiments will begin by conducting a simulation study to determine the viability of the proposed approach. The simulation environment will exist within MATLAB and will allow for several different system parameters to be simulated. We demonstrate that in a wide variety of operating conditions, the overall position error of the daughter-ship is under 3 meters. The overall location accuracy for each parameterized scenario is evaluated and a range of values of which the solution is effective will be determined.

## 1.4 Assumptions/Limitations

The radio that is to be simulated for this research is not yet defined as a real-world radio. It is assumed that there exists a radio which can accurately perform the radio ranging task that is the foundation of this research. This radio is assumed to be

accurate enough to determine the range between the two ships as well as account for any differences in timing between the two systems. It is also assumed that the ships are operating in hostile airspace, with the daughter-ship being GPS-denied whereas the mothership that is GPS-enabled is either resilient enough to resist the GPS denial attempt or is at a distance far enough away to be unaffected.

## 1.5 Thesis Overview

This thesis document is arranged in five chapters. Chapter II provides some background information about some of the technologies that are dealt with in this research, as well as some previous work from the community that is relevant to the research. Chapter III presents the methodology by which the research was conducted and covers topics such as the creation of the simulation space, error calculation, and data generation. Chapter IV presents and discusses the results of the work, and Chapter V summarizes the research and lays out some potential options for future work.

# II. Background and Literature Review

This chapter provides the relevant background subjects and related research that forms the foundation of this thesis work and of which understanding is necessary for later chapters. The chapter begins with a technical summary of some of the technologies used and discussed throughout the work, such as Unmanned Aerial Vehicles, Inertial Navigation Systems, and the Global Positioning System. It also provides a brief overview of the Kalman Filter and Extended Kalman Filter. It follows with a look at related work in the field of GPS denied navigation and some discussion regarding the impact that the works have on this research.

## 2.1 Unmanned Aerial Vehicles

The United States Air Force (USAF) has increasingly relied on UAVs to accomplish its many and varied mission sets. Dependence on UAVs continues to grow as mission sets expand to include tasks such as ISR and combat support. The motivation and idea of the UAV dates back to 1956, when Air Force Major General David Becker stated "We can readily see that except for certain types of missions, the manned combat aircraft will become technically obsolete in the future."[1] Early development of UAVs was conducted by the National Reconnaissance Office (NRO) for intelligence purposes, to be eventually operated in the combat-support role by the USAF in the 1960s. Throughout the Vietnam War era, USAF developed drones flew more than 3,500 combat sorties in a variety of roles. This prompted the Air Force to commit to invest in UAV development in the early 1970s. By the 1980s, the push to counter the Soviet threat had eclipsed the desire for UAV development, resulting in a "UAV Hiatus." The 1990s brought the development of the RQ-1 Predator and RQ-4 Global Hawk, operating the former over Bosnia and Kosovo and breaking some of the

secrecy that had formerly surrounded the systems. By 1999, Predators were handing real-time targeting data to operators in support of Operation Allied Force. The terror attacks of September 11, 2001 as well as the resulting wars in Afghanistan and Iraq brought UAVs into full view of the public. Within a decade, USAF acquisition of UAVs had increased by more than 25-fold - with the Air Force operating over 5,000 UAVs [1].

## 2.2 UAV Navigation

To enable UAV flight, each UAV must be capable of knowing its own state so that it can fly to and observe (or interact with) the correct location and, eventually, land at the correct location. UAVs utilize a suite of sensors, transmitters and receivers to navigate within the world. Typically, UAVs utilize a IMU and GPS receiver to localize themselves. Additional navigation methods can be provided from methods such as visual tracking or computer vision, radio ranging, bearing measurements, or magnetometer readings. The following sections provide a background to commonly used UAV navigation methods.

### 2.2.1 Inertial Navigation Systems

Dr. Charles Stark "Doc" Draper, director of the Massachusetts Institute of Technology Instrumentation Laboratory had been thinking about a project for a long time: "the development of a self-contained inertial navigation system that could provide the pilot with an airplane's location in bad visibility without the assistance of external instruments [2]." Doc approached his government partner and friend, Col Lee Davis of the United States Army Air Forces, to attempt to secure funding for the project. The concept, self-contained Inertial Navigation, would overcome the huge navigation problem experienced by the crews of the Air Forces long range bombers during the

war. The forerunner of modern inertial navigation systems, the Space Inertial Reference Equipment (SPIRE) project, first flew on 9 February 1953. SPIRE's accuracy during the 12-hour, 2,600-mile flight was one one-hundredth of a percent (0.00013). The success of SPIRE gave "credibility to the enormous potential of inertial guidance." [2]

The INS at its core is a dead-reckoning system that calculates vehicle position when given a known starting point. The system functions by utilizing two suites of three sensors measuring both linear and angular accelerations. The first set of three sensors consists of accelerometers aligned orthogonally with the purpose of measuring linear accelerations in each of the vehicle's three translational dimensions. The second set of three sensors consists of gyroscopes aligned orthogonally with the purpose of measuring the vehicle's angular accelerations in the three rotational dimensions. The measurements collected by the accelerometers and the gyroscopes are then integrated in the time domain [3].

The primary advantage of an INS is that it requires no external references in order to determine its position, orientation, or velocity once it has been aligned. The largest limitations of an INS is that the system will exhibit drift, as even the best accelerometers and gyroscopes are subject to noise, biases, and misalignment that gradually increase the total error of the INS position solution. Early inertial systems tended to drift by as much as 15° per hour, with modern electrostatically suspended gyroscopes achieving drift rates of the order of 0.0001° per hour [3]. Even small amounts of drift, however, can drastically impact the performance of a system. The large errors present in early INS systems required an additional aiding instrument to be added to the system to help estimate position and constrain the growth of the error in the INS solution. The initial aiding instrument added to early INS was a stellar sensor, used to correct the accumulated error. The combination of both

systems worked well, if not a little "messy and inelegant" as Doc Draper put it [2]. The practice of aiding an INS with an additional sensor input remains heavily in use today. Most modern day systems utilize GPS as the aiding system.

In general, inertial navigation systems are classified by their intended use and amount of drift they experience during a given time period. These parameters stem from the quality of their accelerometer and gyroscope sensors. Table 1 below details a general guideline of the capabilities and costs of some of the typical inertial sensor grades. Note that the values are approximate, as exact drift rates and costs will vary by manufacturer [4].

### 2.2.2 The Global Positioning System

GPS is a form of a Global Navigation Satellite System (GNSS) that was developed by the United States to provide precision navigation and timing for military, commercial, and civil uses. Early attempts were explored through the Navy TRANSIT system, the Naval Research Laboratory Timation Satellites, and Air Force Project 621B before the GPS Joint Program Office officially formed in 1973. The first GPS satellites, known as Block I, were launched in 1978. GPS is made up of three separate segments: the space segment, the control segment, and the user segment. The space segment is nominally made up of 24 active satellites, of which 21 are operational and three are spares. Recently, however, there have been more than 30 satellites making

Table 1: Grades of INS Systems, Costs, and Errors [4]

| **Grade** | **Price Range** | **Pos. Error** | **Gyro Bias Error** | **Accel. Bias Error** |
|---|---|---|---|---|
| Strategic | > $ 500K | < 0.030 km/h | 0.000 °/h | 0.001 mg |
| Navigation | $ 90K to > $ 130K | < 1.700 km/h | 0.005 to 0.015 °/h | 0.030 to 0.050 mg |
| Tactical | $ 6K to > $ 35K | 18 to 40 km/h | 0.500 to 10 °/h | 0.500 to 1.000 mg |
| Consumer | > $ 350 | > 40 km/h | 1000 °/h | 20 mg |

up the constellation. The satellites are arranged in six orbital planes with (nominally) four satellites per plane. They orbit at an inclination angle of 55° [5].

The control segment consists of the many ground stations that operate and maintain the GPS constellation. Ground antennas, monitoring stations, and tracking stations are located in strategic locations all over the world. The Master Control Station is located at Schriever Air Force Base in Colorado and is tasked with managing the constellation, monitoring the GPS system performance, and calculating the data sent over the navigation message to keep GPS current [6]. The locations of the components of the control segment are shown in Figure 1. The user segment consists of all users of GPS and the receivers that allow for location. Receivers are found in many devices such as cell phones, automobiles, aircraft, spacecraft, and surface ships. GPS receivers are commercially produced and are used in many applications ranging from obvious such as navigation and precision timing, to more obscure such as power grid management and global banking support [5].

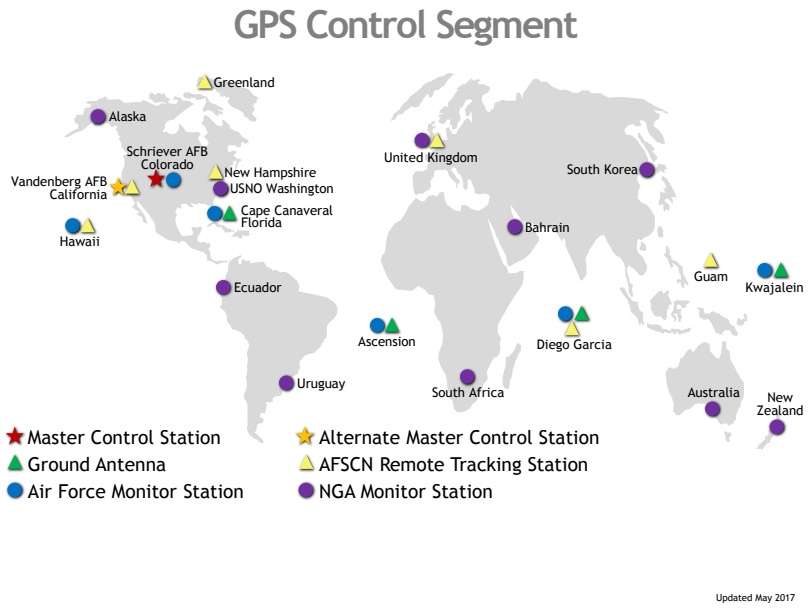


Figure 1: The GPS Control Segment Map [6]

GPS operates through the transmission of Radio Frequency (RF) signals from satellites to receivers within line of sight. Each GPS satellite orbiting in the constellation transmits a unique signal known as a Pseudo-Random Noise (PRN) code and orbital parameters that allow GPS devices to compute the precise location of the satellite. GPS receivers use the satellite location information and trilateration to compute the user's location. Each satellite has its own unique PRN which is transmitted over one of the three carrier frequencies: L1 (1575.42 MHz), L2 (1227.6 MHz) and L5 (1176.45 MHz). PRN codes are transmitted in two classes of code: the coarse-acquisition (C/A) code and the precise (P) code. C/A code and P code differ by the chipping rate, chipping period, and code repeat intervals. C/A code is intended for initial acquisition of the GPS signal, whereas P code provides better performance and more precise positioning. P code is encrypted by an encryption code known as Y code, and is often referred to as P(Y) code. The encryption helps to prevent spoofing of the signal. Also transmitted is the navigation message which contains necessary ephemeris and almanac parameters required to calculate a precise position [5].

Essentially, the GPS receiver measures the distance to each satellite by measuring the amount of time it takes to receive a transmitted signal. The receiver knows the time at which the signal was transmitted, the speed at which the signal travels (the speed of light), and the time at which the signal was received. This method of calculating position is known as code measurement and yields accuracy on the order of 2-4 meters. Typical civilian GPS error averages around 5 meters [7].The second method of calculating position, known as carrier-phase measurement, generates range by counting the number of wavelengths of the carrier signal from transmission to reception. Signal wavelength is known, but calculation of position is more difficult due to ambiguities in the resolution and where in the phase cycle a measurement occurs. Successfully resolving the ambiguities results in accuracy on the order of 1

cm [5]. Certain applications, such as differential GPS, combine both code and carrier phase measurements. After code or carrier phase measurements are received, solving for position is a matter of having a sufficient amount of measurements to resolve a location. Typically, four satellites and their measurements are needed to calculate position and time. Having four satellites accounts for all variables in the pseudorange equation: x, y, z position and receiver clock error.

GPS is a critical tool for precise navigation and timing and forms the backbone of many modern systems. However, GPS is not infallible and has some key limitations that should be understood. GPS relies on RF signals from space which are susceptible to blocking (GPS jamming) or to being altered to make the receiver tell its user that it is in a different location than it actually is (GPS spoofing). Jamming and spoofing are inherent weaknesses in all GNSS systems and can be achieved through various means depending on the prowess of the adversary [8]. For this reason, studies are being conducted to minimize or mitigate the effect of GPS denial and make systems resilient when used in an operational environment that may be GPS denied.

GPS is just one example of a GNSS. Other systems are owned and operated by various countries around the world, including GLONASS, a Russian built GNSS, Galileo, a GNSS operated by the European Union, and Beidou, a GNSS operated by the Chinese. While each system offers similar objectives of precision navigation and timing, the systems differ in the amount of satellites, orbits, and frequencies used [5].

### 2.3 The Kalman Filter

The optimal linear estimator, the Kalman filter, is a recursive data processing algorithm that incorporates "all available measurement data, plus prior knowledge about the system and measuring devices, to produce an estimate of the desired variables in such a manner that the error is minimized statistically [9]." The Kalman

filter requires some assumptions to be effective, which are:

- The system model is linear
- Additive White Gaussian Noise (AWGN) is the only noise present
- All system states are Markov Processes
- The system's initial states are Gaussian

The assumption that all system states are Markov processes means that the value assumed by the current state embodies all information needed for propagation to its next step; essentially that the value of the state depends only on its value at the previous time step and at the current input. The states of the system at the current time represent all previous system states and inputs over time [9]. The future states of the system then follow a Bayesian approach [10]:

$$P(\mathbf{x}_k|\mathbf{z}_k, \mathbf{u}_k) = \frac{P(\mathbf{z}_k|\mathbf{x}_k)P(\mathbf{x}_k|\mathbf{z}_{k-1}, \mathbf{u}_k)}{P(\mathbf{z}_k|\mathbf{z}_{k-1})} \tag{1}$$

Where $\mathbf{x}_k$ is the state vector of the system, $\mathbf{u}_k$ are the inputs to the system and $\mathbf{z}_k$ are the measurements of the system.

### 2.3.1 The Kalman Filter Equations

To determine the state distributions, Equation (1) can be solved by applying the Kalman filter equations recursively in two steps: propagate and update. The Kalman filter propagate equations are defined as follows:

$$\hat{\mathbf{x}}_k^- = \mathbf{\Phi}\hat{\mathbf{x}}_{k-1}^+ + \mathbf{B}\mathbf{u}_k \tag{2}$$

$$\mathbf{P}_k^- = \mathbf{\Phi}\mathbf{P}_{k-1}^+\mathbf{\Phi}^T + \mathbf{Q}_d \tag{3}$$

The state transition matrix, $\mathbf{\Phi}$, defines the relationship of the states between the individual time steps whereas $\mathbf{B}$ defines the relationship of the inputs to the system states. The state vector of the system is fully defined by a mean and covariance, $\hat{\mathbf{x}}_k$ and $\mathbf{P}_k$, respectively. $\hat{\mathbf{x}}_{k-1}^{+}$ is the mean of the system at time *k-1* after the measurement update, notated by the + symbol. $\mathbf{P}_k^{-}$ refers to the system's covariance matrix at the time $k$, before any measurement updates are applied. $\mathbf{Q}_d$ is the discritized system covariance. After propagating the system forward, the next step is to update. The update step incorporates measurement information about the system from the measurement model. The Kalman filter update equations are defined as follows:

$$\hat{\mathbf{x}}_k^{+} = \hat{\mathbf{x}}_k^{-} + \mathbf{K}_k \mathbf{Y}_k \tag{4}$$

$$\mathbf{P}_k^{+} = \mathbf{P}_k^{-} - \mathbf{K}_k \mathbf{H} \mathbf{P}_k^{-} \tag{5}$$

Where

$$\mathbf{K}_k = \mathbf{P}_k^{-} \mathbf{H}^T [\mathbf{H} \mathbf{P}_k^{-} \mathbf{H}^T + \mathbf{R}]^{-1} \tag{6}$$

$$\mathbf{Y}_k = \mathbf{z}_k - \mathbf{H} \hat{\mathbf{x}}_k^{-} \tag{7}$$

$\mathbf{K}_k$ is known as the the Kalman gain whereas $\mathbf{Y}_k$ is the residual of the measurements. After applying the update step, the current system mean and covariance are now once again ready to be propagated. This process is continued recursively. More information about the Kalman filter, as well as a full derivation of the propagate and update equations, can be found in [9].

### 2.3.2 The Extended Kalman Filter

With the Kalman filter, one important assumption was made: the dynamics of the system model are linear. However, this key assumption limits the application of the

Kalman filter in most real world systems as real world systems experience both non-linear process and measurement dynamics. Therefore, a solution is needed to address the linearity assumption to expand the capability of the Kalman filter. One such solution is known as the Extended Kalman Filter (EKF). The EKF is an extension of the Kalman filter estimator for use in a non-linear environment and can handle systems with both linear and non-linear process and measurement models. For the EKF to function, however, the other assumptions must hold true: The states must be Gaussian, Markov processes and noise is still AWGN. If these assumptions remain true, the non-linear functions on the process and measurement models can then be linearized by Taylor Series Expansion about a chosen point. Modified versions of the Kalman filter equations can then be applied. It should be noted that the solution then becomes approximate, meaning that there is no guarantee that the estimates from the filter will be statistically minimized errors. This renders the EKF a sub-optimal filter, mathematically, but has still shown acceptable results in hundreds of applications. The EKF equations are as follows [11] [12]:

**Extended Kalman Filter Propagate Equations**

$$\hat{\mathbf{x}}_k^- = f(\hat{\mathbf{x}}_{k-1}^+, \mathbf{u}_k) \tag{8}$$

$$\mathbf{P}_k^- = \tilde{\mathbf{\Phi}}_{k-1}\mathbf{P}_{k-1}^+\tilde{\mathbf{\Phi}}_{k-1}^T + \mathbf{Q}_d \tag{9}$$

**Extended Kalman Filter Update Equations**

$$\hat{\mathbf{x}}_k^+ = \hat{\mathbf{x}}_k^- + \mathbf{K}_k\mathbf{Y}_k \tag{10}$$

$$\mathbf{P}_k^+ = (\mathbf{I} - \mathbf{K}_k\tilde{\mathbf{H}}_k)\mathbf{P}_k^- \tag{11}$$

Where

$$\mathbf{K}_k = \mathbf{P}_k^- \tilde{\mathbf{H}}^T [\tilde{\mathbf{H}} \mathbf{P}_k^- \tilde{\mathbf{H}}^T + \mathbf{R}]^{-1} \tag{12}$$

$$\mathbf{Y}_k = \mathbf{z}_k - h(\hat{\mathbf{x}}_k^-) \tag{13}$$

$\mathbf{K}_k$ and $\mathbf{Y}_k$, the Kalman gain and measurement residual, remain the same. The Kalman filter equations use the linear terms $\mathbf{\Phi}$ and $\mathbf{H}$ described by Equation (14) and Equation (15), whereas the EKF uses the Jacobian of the $f$ and $h$ functions, respectively.

$$\mathbf{\Phi}_k = \left. \frac{\delta f(\mathbf{x}, \mathbf{u})}{\delta x} \right|_{x=\hat{\mathbf{x}}_k^+, \mathbf{u}_k} \tag{14}$$

$$\mathbf{H}_k = \left. \frac{\delta h(\mathbf{x})}{\delta x} \right|_{x=\hat{\mathbf{x}}_k^-} \tag{15}$$

For more information about the EKF, see [9], [11] and [12].

### 2.4 Related Work in GPS Denied Navigation

Work has been accomplished on other, alternative methods of navigation that do not require GPS. Methods such as visual tracking or computer vision, radio ranging, bearing measurements, or magnetic navigation provide alternative methods of localizing the aircraft in the absence of GPS. These methods will be described in the subsections below. While these methods do have the benefit of adding navigation resiliency to the aircraft, they have their own set of challenges and disadvantages to contend with. Note that the methods mentioned are not all-inclusive or necessarily standalone, meaning research on other methods or combination of methods may exist to help localize aircraft in the absence of GPS.

### 2.4.1 Vision Aided Navigation

Vision aided navigation is an alternative navigation method that utilizes one or more cameras on the UAV to obtain vehicle pose information during a GPS outage. Navigation using a camera is appealing because the typical UAV already carries a camera, either for remote piloting or surveillance. Typical vision aided navigation approaches can be broadly categorized into two methods: 1) methods that rely on identifying features in the scene, and 2) methods that use only registered models of the environment [13]. Images from the camera can be processed to create lines of sight to landmarks or features that can then be identified. The lines of sight can be used to triangulate the pose of the camera, and thus the vehicle [14]. The first approach uses feature tracking that can only provide partial navigation aiding. The second approach can achieve full localization, but requires a registered model of the environment. The models can be derived from man-made structures or natural features. The main disadvantage for vision aided navigation is the differences that may occur between reference imagery and operational conditions that can effect system performance. For example, weather (cloud cover, snow, rain) could cause the environment to be suitably altered to the point at which the features or landmarks no longer properly register as such and therefore do not allow for localization. Vision methods have the potential to augment the ranging work described in this thesis research, but are not included in the scope of this work.

### 2.4.2 Navigation Using Bearing Measurements

Another type of alternative navigation is the use of bearing measurements to localize a GPS-denied aircraft. This approach is similar to navigation using radio ranging, the key difference being the measured quantity is bearing instead of range. Prior works have explored the use of bearing measurements as a replacement or aide

for GPS. Research performed by Zhang, Ye, Anderson, Sarunic, and Hmam, attempts to cooperatively use bearing measurements to navigate in a GPS-denied environment. The work assumes that multiple UAVs exist in a two-dimensional space: at least one with GPS, and others that are GPS-denied but are INS-enabled. The GPS-equipped vehicle broadcasts its global coordinates to the GPS-denied vehicles and the GPS-denied vehicles also obtain a bearing measurement to the GPS-equipped vehicle. By obtaining four or more measurements between at least two UAVs, localization of a GPS-denied vehicle in the global coordinate frame is possible. Additional special cases are examined like the performance when noise is added to the measurements as well as some bearing ambiguities such as a stationary ship or bearings of equal value [15]. This approach has a few key assumptions, namely that the ships are operating in a two-dimensional space and that the bearing measurements are free of noise. Additional related work involves cooperative navigation of Miniature Air Vehicles (MAVs) using bearing measurements. In the work performed by Sharma and Taylor, each MAV in a swarm estimates position, attitude, and velocity of all MAVs in sensor range including itself. These measurements are then fused with relative range and bearing measurements, and that data is used in an EKF to estimate the navigation states [16]. This prior research differs from this thesis in a few key ways:

- The prior work involves multiple UAVs, where this thesis considers just two
- Prior work was restricted to two-dimensions while the simulations in this thesis utilize a three-dimensional world
- This thesis considers range-only measurements, without bearing

### 2.4.3 Magnetic Navigation

Magnetic anomaly navigation is a method of analyzing the magnetic field in the local area and cross-referencing it with known magnetic field strength data to localize oneself. The technique is not GPS dependent and has been shown to have been accurate to tens of meters over both land and water [17]. In order to obtain the maps needed for this method, an aircraft must fly in a close set of parallel flight lines over an area of interest. The aircraft collects intensity data using high resolution magnetic sensors, of which the data is analyzed and magnetic fluctuations due to the collection platform are compensated for. Another type of mapping of magnetic anomaly data is the collection of magnetic vector data, which is substantially more difficult than collecting intensity data. This data must be collected using high quality, extremely sensitive sensors and must be collected using very precise attitude accuracy [17]. In Hardy et al's research into UAV navigation in GPS denied environments, magnetometer readings are one source of data discussed to obtain localization of the UAV. The research assumes an identical magnetic field vector acting on both aircraft as they are in close proximity. Using this assumption, the relative attitude between the two platforms is used to rotate the body axis magnetometer data from one platform to the other. Then, the magnetometer sensor data is used to make a comparison between the two platforms which helps to minimize the drift in the INS [18]. These methods do have a few drawbacks, however. First and foremost, the area in which the aircraft are operating must have been mapped. As Canciani and Brennan mention, the collection of high quality magnetic field vector data on airborne platforms is substantially more difficult than collecting intensity data as well as more expensive [17]. Additionally, research has focused on using this type of sensing as an aide to other GPS-denied navigation methods rather than a single solution. While this solution is extremely resilient, the accuracy of the position solution is currently

on the order of tens of meters which is unacceptable for precision navigation uses.

### 2.4.4 Navigation Using Radio Ranging

Navigation through the usage of radio ranging is the primary method of GPS-denied navigation that was explored for this thesis work. There is some previous work on the topic with various assumptions that set conditions on the real-world application of such methods. Navigation using radio ranging is a method which uses the on board navigation system and ranging radio to estimate the relative pose of an aircraft in flight. Most applications require two or more moving aircraft and multiple measurements to resolve ambiguities when calculating position using the ranging measurements. Additionally, much of the available research incorporates navigation methods other than the radio ranging to provide a more precise position solution.

In their approach, Strader, Gu, Gross, De Petrillo, and Hardy use a pair of UAVs with on board INS and a ranging radio to estimate the relative pose of each UAV using a single range measurement. This is conducted in a two-dimensional environment, or co-altitude, using motion to augment the limited amount of information available. A graph is formed from the range measurements and displacement in position over time, and the analytical solution is derived from the constructed graph. The approach is also assumed to be noise free. Figure 2 shows the approach graphically. $A$ and $B$ are the two systems, where the position of each system is denoted by $A_1$, $A_2$, ..., $A_n$ for platform $A$ and $B_1$, $B_2$, ..., $B_n$ for platform $B$ where $n$ is the total number of locations. The displacement in distance is between locations is $d_{A1}$, $d_{A2}$, ..., $d_{An-1}$ for platform $A$ and $d_{B1}$, $d_{B2}$, ..., $d_{Bn-1}$ for platform $B$ [19].

The relative pose between the platforms can be obtained by modeling the system as a series of mechanical linkages with rigid links and joints. More information about

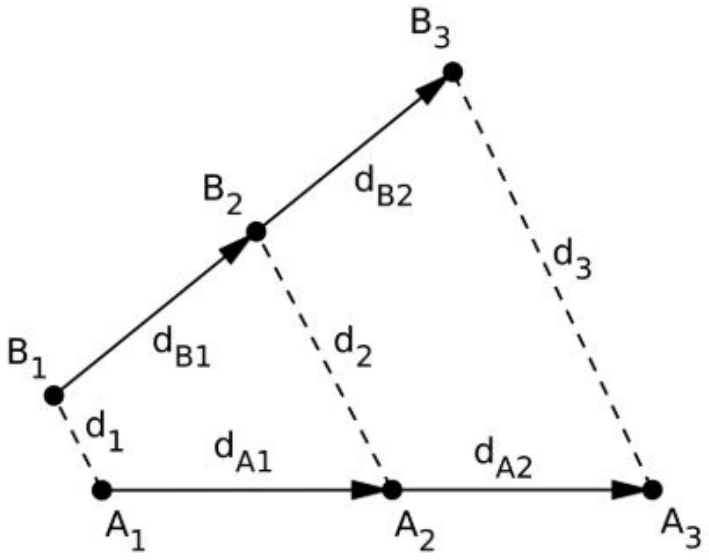


Figure 2: Graphical representation of radio ranging approach [19]

solving this system of equations can be found in [19]. As mentioned in the paper, with sufficient information four possible solutions are obtained for the relative position of platform $B$, two solutions for relative bearing and two solutions for relative position. Weights are assigned to each solution, and this information is stored in memory. Platform $A$ then turns to a different heading and the residual distances are calculated. The system weights are determined and in a noise free system, one solution's weight will approach infinity. Also examined are four special cases which emerge depending on the geometry and path of the platforms.

1. There is one unique solution for the position if the platforms are traveling along the same line in opposing directions.

2. There are two solutions for the position if the platforms are traveling parallel to each other with different velocities.

3. There are four possible solutions for the position if the platforms travel along

intersecting lines.

4. There are an infinite number of solutions for the position if the platforms are travelling parallel to each other with equal velocities.

Conclusions include that the frequency of the measurement impacts the error more than the flight geometry. The approach taken in the aforementioned research differs from this thesis research in a couple of ways. First, the research conducted by Strader et al. assumes two UAVs performing cooperative navigation with no prior or outside navigation information, whereas the thesis research is a mother-daughter ship configuration with the mothership being GPS enabled. Additionally, the thesis research is conducted in three dimensions instead of two.

Ranging radio estimates are also mentioned in the research performed by Hardy et al. on UAV navigation in GPS denied environments. This research takes a similar approach to the research performed by Strader et al., in which a peer-to-peer ranging radio solution is utilized to form the "mechanical linkage" model. The model is then used to estimate position using an EKF. This research primarily focuses on fusing multiple solutions into one resilient approach. The ranging measurements are used, along with IMU measurements, magnetometer readings, and computer vision. This approach assumes cooperative navigation between two UAVs and that both are GPS-denied. A graphical representation of this approach is seen in Figure 3 [18].

In Figure 3, platform $A$ is assumed to be the UAV which is tracking a target whereas platform $B$ is having the target handed off to it. In this example, both systems are assumed to be equipped with a downward facing camera, a peer-to-peer radio ranging system, a tri-axial IMU system, and magnetometer sensors. No prior information about the relative pose of each platform is needed. The mechanical linkage model seen in the work performed by Strader et al. is used to construct a graph with the range measurements between platforms and distance travelled over

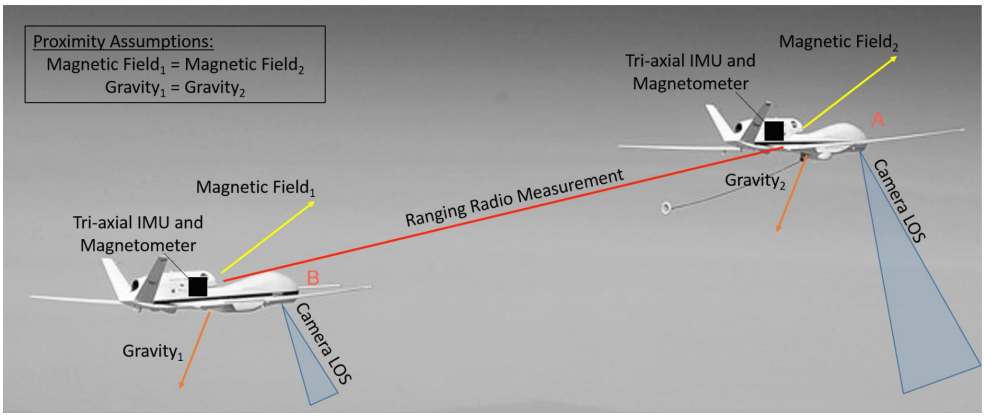


Figure 3: UAV Cooperative Navigation Approach [18]

time [19]. An example can be seen in Figure 4.

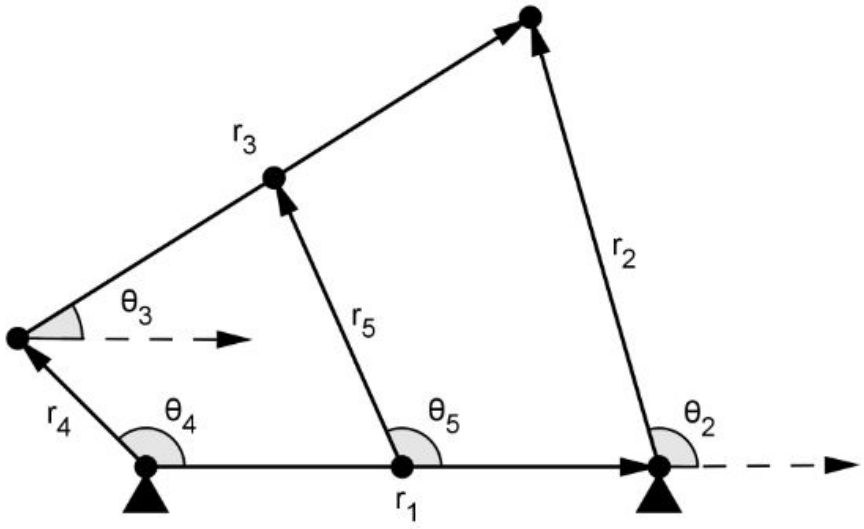


Figure 4: Trajectories of platforms $A$ and $B$ over time [19]

The four "special cases" from the research are examined, particularly the case in which the platforms are travelling along intersecting lines and the case in which the platforms are travelling along parallel lines but have different velocities. The possible solutions are obtained from solving the loop closure equations of the linkage.

$$\alpha \cos \theta_3 = \beta \tag{16}$$

$$\alpha \tan^2(\theta_2/2) + b \tan(\theta_2/2) + c = 0 \tag{17}$$

In Equation (16), $\alpha$ and $\beta$ are constant and are a function of the link lengths. In Equation (17), $a$, $b$, and $c$ are constant and are a function of the link lengths and $\theta_3$ from Equation (16). By substituting in values from the ranging radio measurements and distances, Equation (16) and Equation (17) can be solved. This is assumed to be noise-free. When noisy measurements are used, the equations are solved using the linear least squares method and are then smoothed. An EKF is used to predict the relative pose and angular coordinates for updating the measurements. When the filter converges, then one of the two platforms turns to a different heading and travels at a constant speed. Using the estimate, the position is propagated using the INS and the difference between the radio ranging measurement and the predicted distance can be calculated. The likelihood of the solution is weighted and the solution with the highest likelihood is selected [19].

The radio ranging approach is then combined with measurements and calculations from computer vision and magnetometers. More information about the calculation and usage of that data can be found in [18]. The results of this study show that in GPS-denied cases, position accuracy is on the order of 10-meter-level and degree accuracy is on the order of 0.5 degree-level. It was also shown that the magnetometer measurements had little impact on the overall performance of the algorithm. The work done by Hardy et al. provides a foundation that ranging measurements combined with a Kalman Filter can provide useful and accurate positioning. Their work incorporates additional sensors such as the computer vision sensors and magnetometer to achieve better accuracy. The thesis research described in this document takes

this foundational work and narrows the scope, focusing only on providing accurate measurements using the ranging sensor alone but in the case when one of the two platforms has GPS.

# III. Methodology

This research seeks to utilize the ranging radios of the mothership and daughter-ship to provide a position solution when the daughter-ship is operating in a GPS-denied environment. In order to evaluate the viability of this potential solution, a simulation environment was created and utilized within MATLAB that tests the principles of the approach. This research focuses on using the platform's onboard inertial sensors, with just the ranging radio information passed between platforms and the movement of the platforms as the information to allow the algorithm to work.

This chapter will cover the methodology used in testing the radio ranging approach. The simulation parameters, platform data generation, and governing models of motion will be discussed. This chapter also provides mathematical and graphical verification for the described methodology. The results of the experiments are presented in Chapter IV.

## 3.1 Simulation Overview

The simulation is built in MATLAB and contains two ships, the mothership and daughter-ship which will be referred to as Ship 1 and Ship 2 respectively. Each ship completes orbits with Ship 1 orbiting around the origin and Ship 2 orbiting around a point specified by setting a desired separation distance variable. The two ships behave according to their measurement models and editable parameters, which are described in more detail in the sections that follow. The general idea behind the ships in the simulation space is seen in Figure 5.

The parameters for each ship are set individually at the beginning of the simulation run and remain constant throughout the run. As the two ships move through the

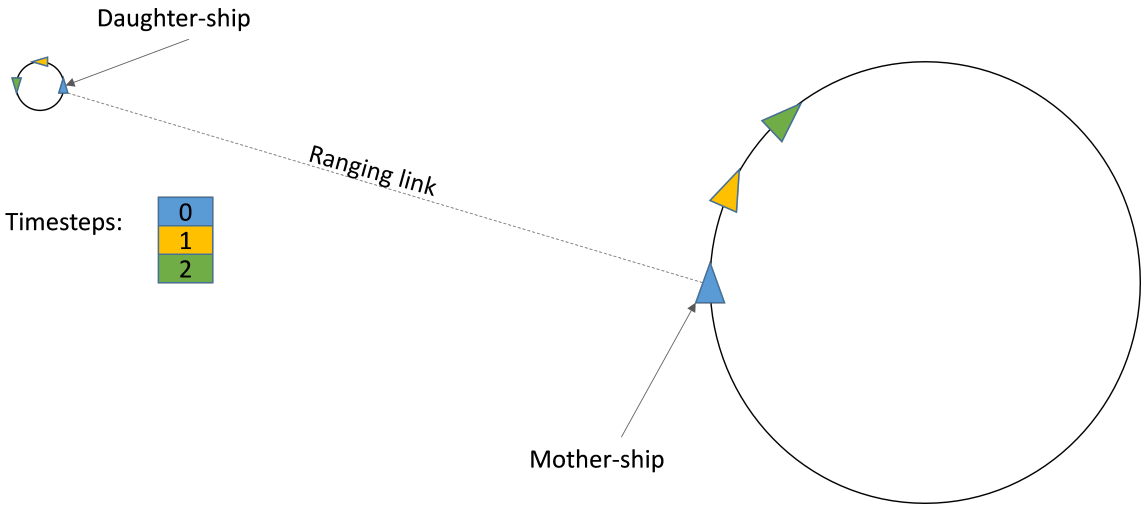


Figure 5: Overview of the simulation, showing the principle behind recovering the geodetic location of Ship 2 when it is GPS-denied.

simulation space, the distance between them changes and this data is then fed into an EKF to estimate the position of Ship 2 based on the input data of the range between the two platforms. A typical simulation run produces a graphical output of the run post-calculation and is not drawn in real-time. The data in the output image includes the path of both ships as well as the EKF's prediction of the position of Ship 2 based on the input data of the range between the two platforms. Data output from the simulation is in the form of the amount of error between the predicted solution and known truth data. A typical output plot is shown in Figure 6.

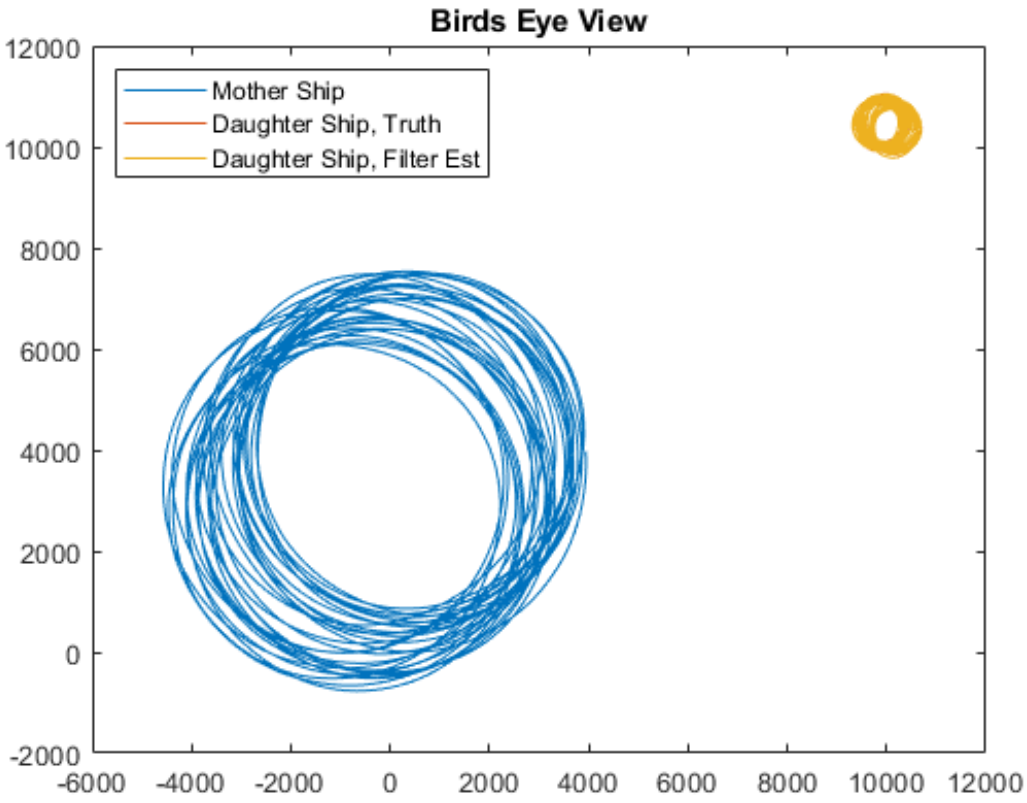


Figure 6: Output figure (bird's eye view) from the simulation. The blue spiral is the path taken by Ship 1, whereas the red spiral is the path taken by Ship 2 during the simulation. The yellow spiral is the EKF's estimation of the position of Ship 2. For this example, the estimation of the filter completely covers the path of Ship 2 which lies underneath the yellow spiral.

### 3.2 Assumptions

The following assumptions are made when designing and executing the experiments within the simulation space:

- Ship 1 is GPS-enabled and is geographically separated from the GPS-denied Ship 2.
- Both ships have a functioning INS.
- The parameters of each ship's flight such as altitude, airspeed, and roll angle

remain constant throughout the simulation.

- The ranging link is available to both ships and is not jammed or denied.
- The ranging sensor is able to achieve expected accuracy, as well as operates independently of GNSS functions and does not rely on those systems for precision timing.

### 3.3 Measurement Model

Both ships have identical equations of motion that govern their movement in the simulation space. As previously mentioned, parameters such as altitude and airspeed are assumed to be held constant. Velocity ($V$) and the roll angle of the aircraft ($\phi$) are the control inputs that define the movement of the ships in the simulation environment. The state vector of the aircraft is $x$, $y$, and heading ($\psi$). The dynamic equations of motion below are adapted from work by Nelson, Barber, McLain, and Beard and are used for the simulation of both ships [20]. It should be noted that the measurement models are subjected to random noise in order to better simulate a real-world environment.

$$\dot{x} = V \cos \psi \tag{18}$$

$$\dot{y} = V \sin \psi \tag{19}$$

$$\dot{\psi} = \frac{g}{V} \tan \phi \tag{20}$$

### 3.4 Simulation Parameters

The simulation environment allows for multiple variables to influence the motion of the ships as well as the performance of the filter. The subsections that follow

describe the parameters that can be set and how they affect the performance of the simulation.

### 3.4.1 Simulation Constants

Certain parameters affect the behavior of the simulation but are not changed during testing. The parameters are able to be changed to fit the desired performance of the simulation but are kept constant for the purposes of this research. These constants include the force of gravity, length of the simulation, and sampling rate of the simulation. The values used in the simulation are shown in Table 2.

Table 2: Simulation Constants

| **Parameter** | **Value** |
|---|---|
| Gravity | 9.81 $m/s^2$ |
| Length (seconds) | 5,000 |
| Sampling Rate (samples/second) | 100 |

### 3.4.2 Testing Parameters

The following parameters are changed during testing to observe the effect that the parameter has on filter performance and accuracy. Values were selected with the intention of being reasonable and realistic for the proposed operational aircraft. Ship 1 was modeled to be similar to an AC-130U gunship [21] and Ship 2 was modeled to be similar to the ALTIUS-600 UAV [22]. The parameters tested in the simulation and the range over which they were tested is shown in Table 3.

Table 3: Simulation Variable Parameters

| **Parameter** | **Test Range** |
|---|---|
| Velocity, Ship 1 | 75 m/s - 150 m/s |
| Velocity, Ship 2 | 5 m/s - 30 m/s |
| Roll Angle, Both Ships | -50° - 50° |
| Altitude, Ship 1 | 100 m - 10,000 m |
| Altitude, Ship 2 | 50 m - 3,000 m |
| Separation Distance | 500 m - 100,000 m |
| Range Sensor Noise | $0.001^2$ - $2^2$ |
| IMU Uncertainty, Ship 2 | $0.00001^2$ - $0.02^2$ |

### 3.5 Error Calculation

Error is the main metric that is measured in this work. The error is defined as the difference between the known truth data of Ship 2 and the predicted values that are calculated by the filter in both the $x$ and $y$ directions. Experiments performed in this work use root-mean-square error (RMS error) to appropriately display the accuracy of the position solution. RMS error is computed for both $x$ and $y$ sources of error. RMS error is calculated according to Equation (21), where $n$ is the number of measurements, $\hat{p_{x,y}}$, $p_{x,y}$ are the estimated and truth values of Ship 2 in the $x$ and $y$ directions at position $p$, respectively [23].

$$RMS\ Error = \sqrt{\frac{\sum_{n}^{p=1}(\hat{p_{x,y}} - p_{x,y})^2}{n}} \tag{21}$$

### 3.6 Data Generation

The simulation is run using pre-generated data based on the measurement model and parameters. Data must be generated before being used by the EKF. The data generation process follows the following steps:

1. Desired simulation parameters are defined by the user and saved as a .mat file to be loaded as a model.

2. Model parameters are loaded and truth trajectories are generated for both Ship 1 and Ship 2.

3. Trajectories are corrupted with noise to better simulate real-world environment.

4. Range is calculated and saved as a variable in the workspace. Range takes into account distance and altitude differences.

5. Range measurement is corrupted with noise to better simulate real-world environment.

After the data is generated and stored in the workspace, then the EKF can access it and the simulation may run.

### 3.7 Experimental Design

Following data generation, the filter is run and results are recorded. The experiments are conducted with two primary goals in mind. The first goal is to determine the viability of using ranging measurements to correctly determine the location of Ship 2 when operating in a GPS-denied environment. Once this capability is shown to be viable the next goal is to determine the effect of the simulation parameters on the accuracy of the position solution. To accurately determine the effect that the individual parameters have on the overall performance of the filter and accuracy of the position solution, a baseline simulation is created and the results are recorded. The values of the baseline simulation are described in Table 4.

The experimental procedure then follows by selecting one parameter and making changes to the value while the remainder of the parameters remain set to the baseline values. This allows for an accurate determination of the effect that the individual parameter has on the performance of the entire system. The tested values are evenly distributed across the testing range mentioned in Table 3. For the parameters of

Table 4: Simulation Baseline Parameters

| **Parameter** | **Baseline Value** |
|---|---|
| Velocity, Ship 1 | 125 m/s |
| Velocity, Ship 2 | 15 m/s |
| Roll Angle, Ship 1 | 25° |
| Roll Angle, Ship 2 | 5° |
| Altitude, Ship 1 | 3000 m |
| Altitude, Ship 2 | 500 m |
| Separation Distance | 10,000 m |
| Range Sensor Noise | $0.1^2$ |
| IMU Uncertainty, Ship 2 | $0.01^2$ |

velocity, roll angle, and altitude, 100 combinations of tests were performed to get an accurate representation of the test space. This corresponds to 10 evenly spaced test parameters across Ships 1 and 2 and all permutations of those values. For the parameters of separation distance, range sensor noise, and IMU uncertainty, the testing space was evenly distributed into 20 values to be tested. This allowed for a more thorough examination of the testing space with acceptable resolution between test values.

Each test is run 50 times in order to capture enough data to be representative of the performance of the simulation. The RMS error from each run is collected and stored and the average of the 50 tests is then taken. The results are recorded and stored in a .mat file for analysis and plotting, which is discussed the the corresponding results section. This process is repeated for all parameters to be tested.

# IV. Results and Analysis

## 4.1 Overview

This chapter describes the results obtained from testing the parameters described in Chapter III within the simulation. The baseline results are discussed first and subsequent parameters are discussed as they relate to the change from the baseline performance. Results are displayed in multiple formats. First, results are shown in numerical form in a table. Error values are displayed for both $x$ and $y$ as well as the root-sum-square error. For parameters where a range of values are tested, a maximum and minimum error value are shown. Results of all tests are shown in full in Appendix A. Results are also shown graphically, either as a depiction of the path taken by the two ships for the baseline model or as surface plots for individual parameters that are tested.

## 4.2 Baseline Simulation Results

This section analyzes the feasibility and accuracy of the approach by comparing the baseline model results to the known truth data. The simulation is configured with the parameters set according to Table 4 in Chapter III. Note that the simulation was run for 50 iterations and the associated error values were averaged across the runs. Table 5 provides the results from the baseline experiment tests.

Table 5: Simulation Baseline Results, 50-Run Average

| **Description** | **Value** |
|---|---|
| Average X Error | 0.936 m |
| Average Y Error | 1.193 m |
| Average Total Error | 1.516 m |

The baseline simulation averages out at 1.516 meters of error across the 5,000

second long testing range. Figure 7 and Figure 8 show the performance of the filter, with Figure 7 showing the overview from a distance whereas Figure 8 shows a close-up of the behavior of Ship 2.

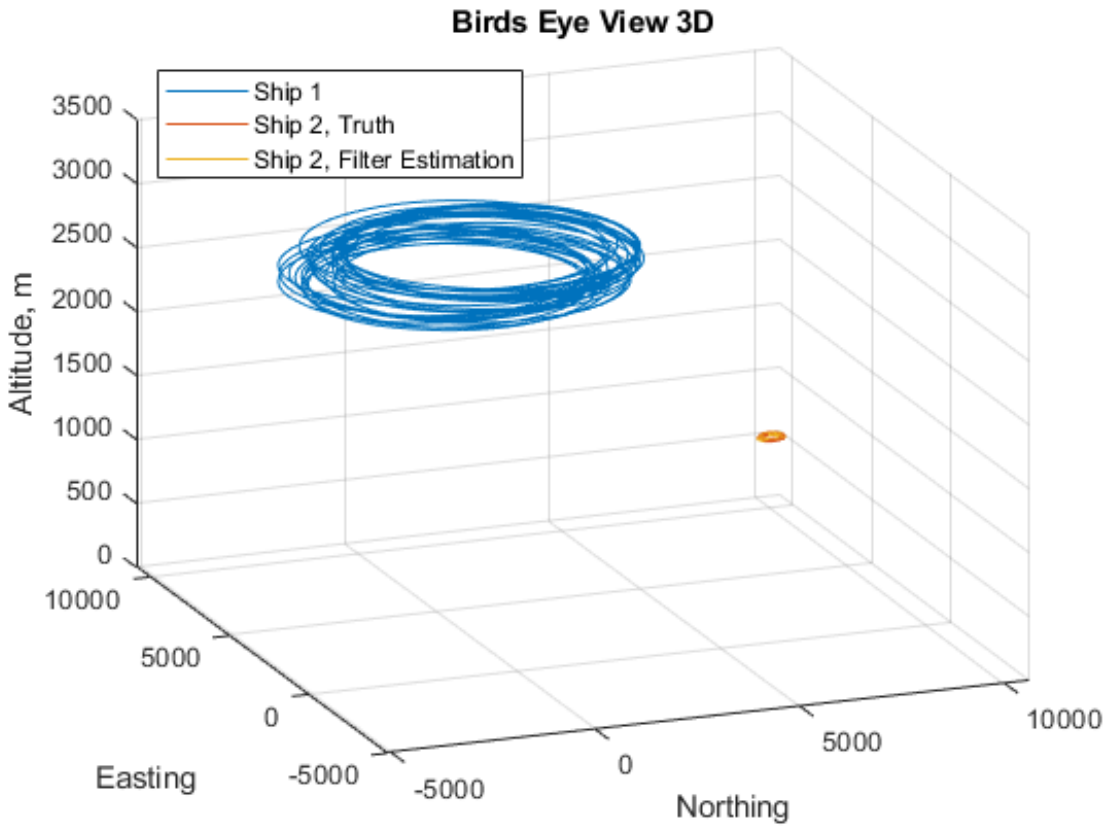


Figure 7: Performance of the baseline model. Ship 1 is in blue, the truth data for Ship 2 is in red and the filter estimation of Ship 2 is in yellow.

Figure 9 shows the distribution of the error values of the baseline simulation. Error values range from 1.0 to 2.0 meters of error, with the majority of the runs providing results within the range of 1.4 to 1.5 meters of error. The differing results are due to the addition of random noise to the parameters. These results indicate that the simulation is functioning properly and does not have large outliers in the data.

Note that these results fulfill our first objective of ensuring that the ranging measurements can be used to replace GPS in the mothership/daughter-ship scenario

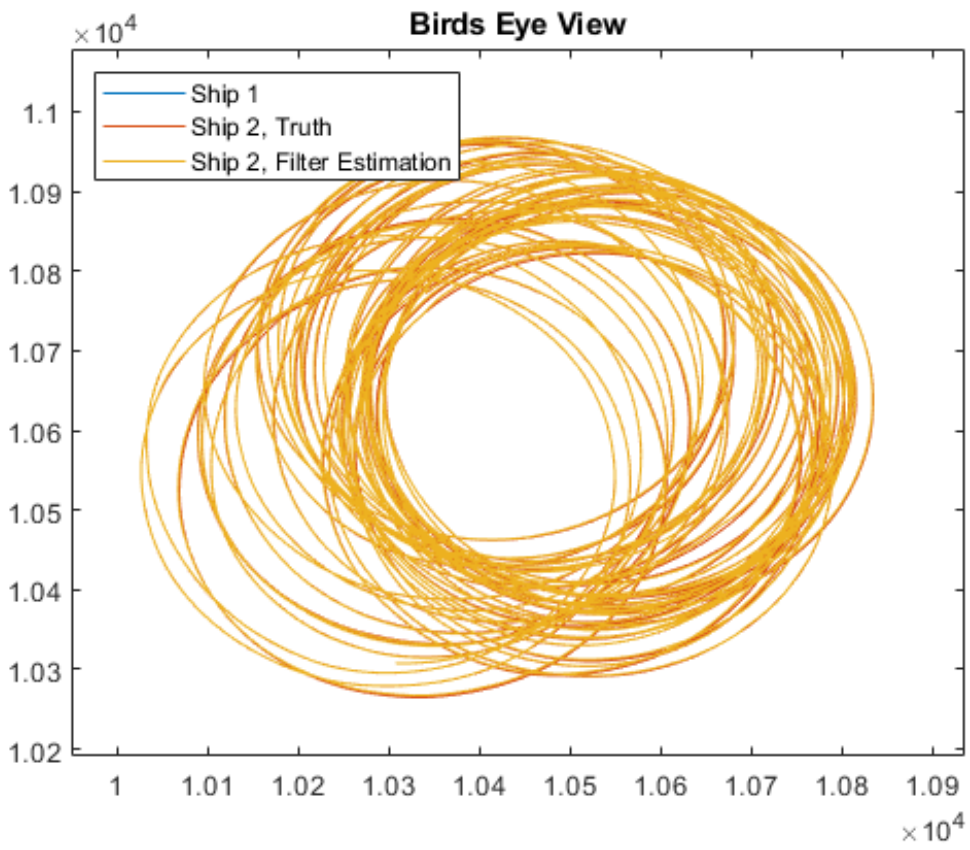


Figure 8: Performance of the baseline model, zoomed on Ship 2. The truth data is in red and the filter estimation of position is in yellow. The estimation is very close to the truth data indicating a well operating filter.

described in Chapter I. Notice that the results described in Table 5 are less than 2 meters of error. Furthermore, Figure 7 and Figure 8 show graphically that the filter estimation is very close to the truth data of Ship 2. This indicates a well operating filter and serves as the reference performance for the rest of the tests performed. The path of the ships does not follow perfect orbits due to random noise present in the parameters in order to provide a better approximation of operation in a real-world environment.

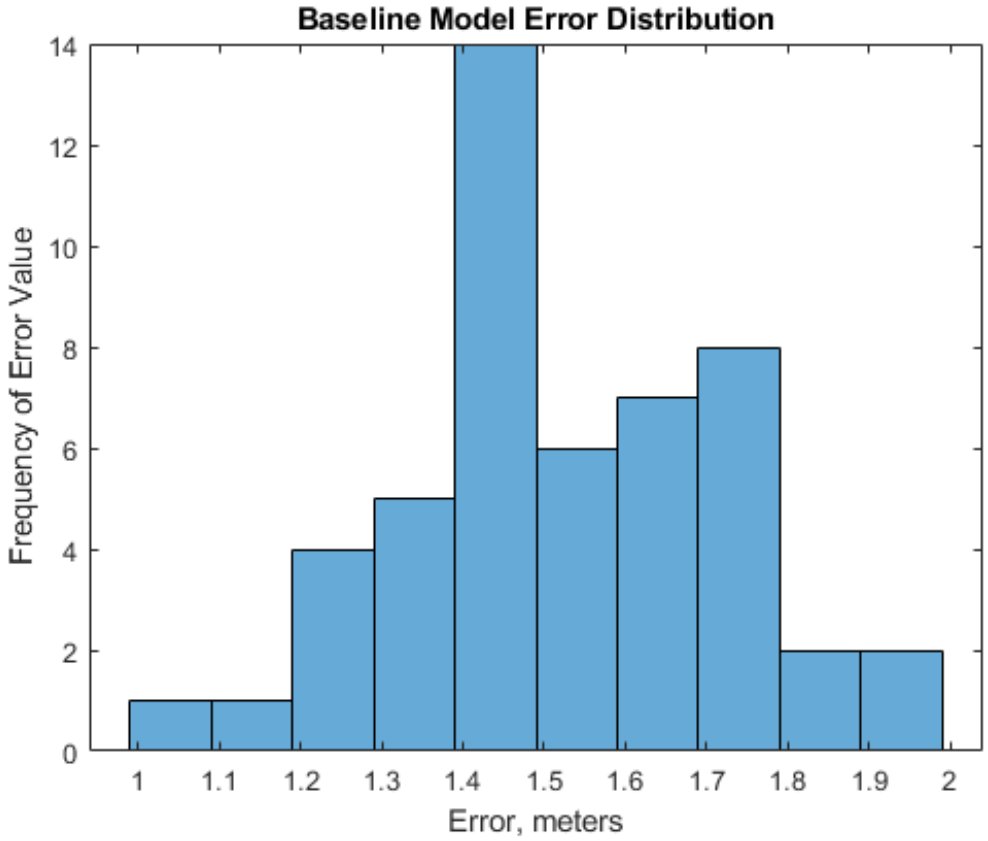


Figure 9: Histogram showing the distribution of the error values of the baseline simulation. Error values fall in the range of 1 meter to 2 meters, with the majority of the runs falling between 1.4 and 1.5 meters of error.

### 4.3 Effects of Varied Velocity Values

The velocity of the two ships has a moderate impact on the error between the truth and predicted values. The tested values of Ship 1 velocities ranged from 75 meters per second to 150 meters per second and Ship 2 values ranged from 5 meters per second to 30 meters per second. Table 6 provides the numerical results from the velocity experiment tests. Note that the error values are the maximum, minimum, and average error results obtained from a 50-run average. Figure 10 and Figure 11 show surface plots of the velocity experiment tests, plotting Ship 1, Ship 2, and X and Y error, respectively.

Table 6: Velocity Simulation Results, 50-Run Average

| **Description** | **Value** |
|---|---|
| Minimum X Error | 0.393 m |
| Maximum X Error | 3.345 m |
| Average X Error | 1.371 m |
| Minimum Y Error | 0.587 m |
| Maximum Y Error | 3.559 m |
| Average Y Error | 1.573 m |
| Minimum Total Error | 0.706 m |
| Maximum Total Error | 4.954 m |
| Average Total Error | 2.088 m |

It is seen that the X-error and Y-error plots are nearly identical, and the values seen in Table 6 reflect this fact. Values range from sub 1 meter error on the lower end to over 5 meters of error on the upper end. The performance is tied more to Ship 2's velocity, trending upward as the velocity of the ship increases. Ship 1's velocity has little impact on the performance of the filter. This is likely due to the orbiting behavior of the ships in the simulation. As the velocity of Ship 2 increases, the orbits become larger and farther apart. This results in more erroneous position estimations as the distance measurements are spread out more and therefore do not change as rapidly.

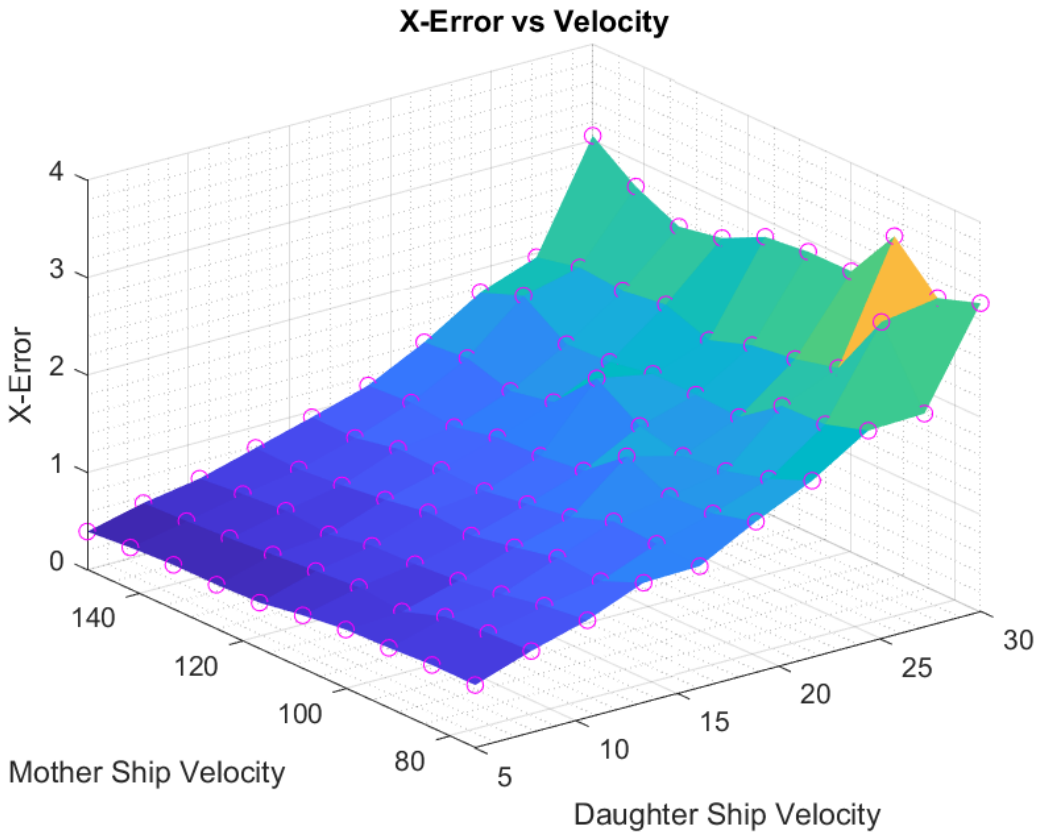


Figure 10: Surface plot comparing ship velocities to X-error. The circles, in purple, show the individual data points which make up the surface mesh.

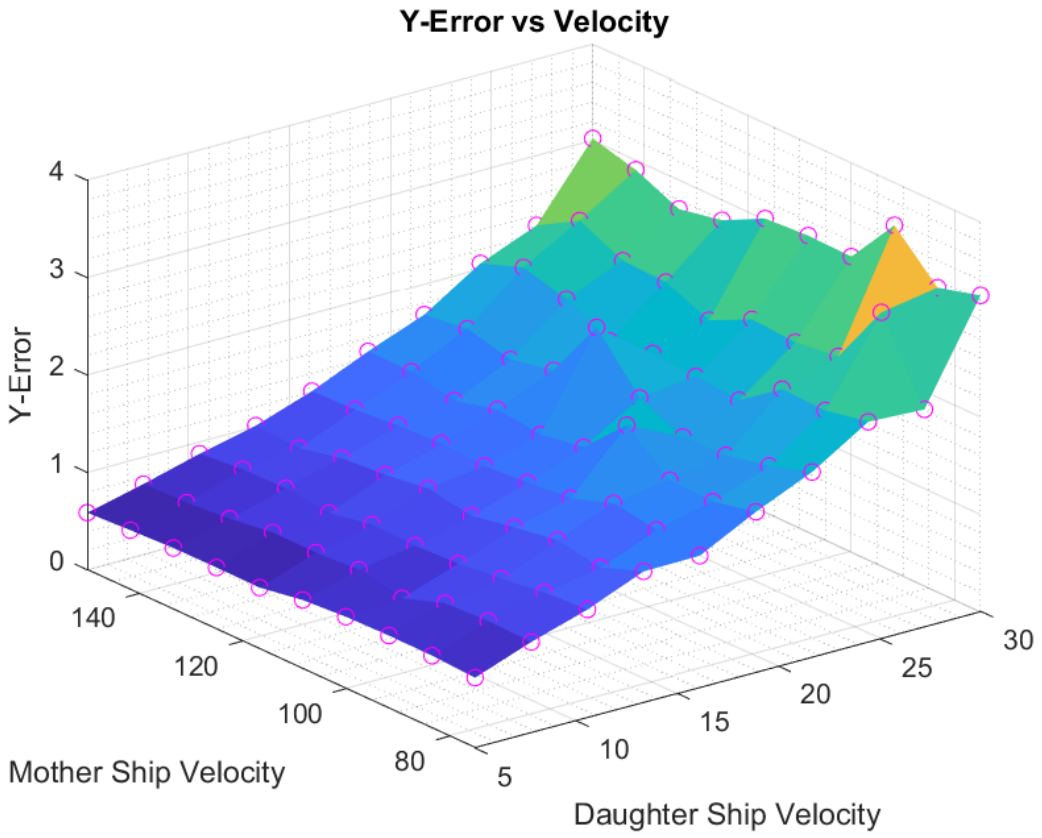


Figure 11: Surface plot comparing ship velocities to Y-error. Nearly identical to the X-error plot, the Y-error is slightly higher overall.

### 4.4 Effects of Varied Roll Angle Values

The roll angle of the two ships has little impact on the error. The tested values of both ships roll angles were from -50° to 50°. Table 7 displays the numerical results from the roll angle experiment tests. Note that the error values are the maximum, minimum, and average error results obtained from a 50-run average. Figure 12 and Figure 13 show surface plots of the roll angle experiment tests, plotting Ship 1, Ship 2, and X and Y error, respectively.

Table 7: Roll Angle Simulation Results, 50-Run Average

| **Description** | **Value** |
|---|---|
| Minimum X Error | 0.639 m |
| Maximum X Error | 1.817 m |
| Average X Error | 1.119 m |
| Minimum Y Error | 0.826 m |
| Maximum Y Error | 1.746 m |
| Average Y Error | 1.058 m |
| Minimum Total Error | 1.221 m |
| Maximum Total Error | 2.239 m |
| Average Total Error | 1.558 m |

The values shown in Table 7 illustrate that the roll angle of the two platforms does not have much of an effect on the error between the truth and predicted values of Ship 2. All error values fall below 3 meters, with minimums below 1 meter. It should be noted that this analysis purposefully avoids the roll angle of zero degrees for both platforms. The algorithm depends on the range measurements changing over time, therefore having the ships at zero degrees of roll angle breaks the method. This is especially important for Ship 2, which is making smaller orbits than Ship 1. Although zero degrees is avoided, the behavior still begins to exhibit itself when approaching zero degrees. This can be seen in Figure 12.

As previously mentioned, error begins to increase around the zero degree line and

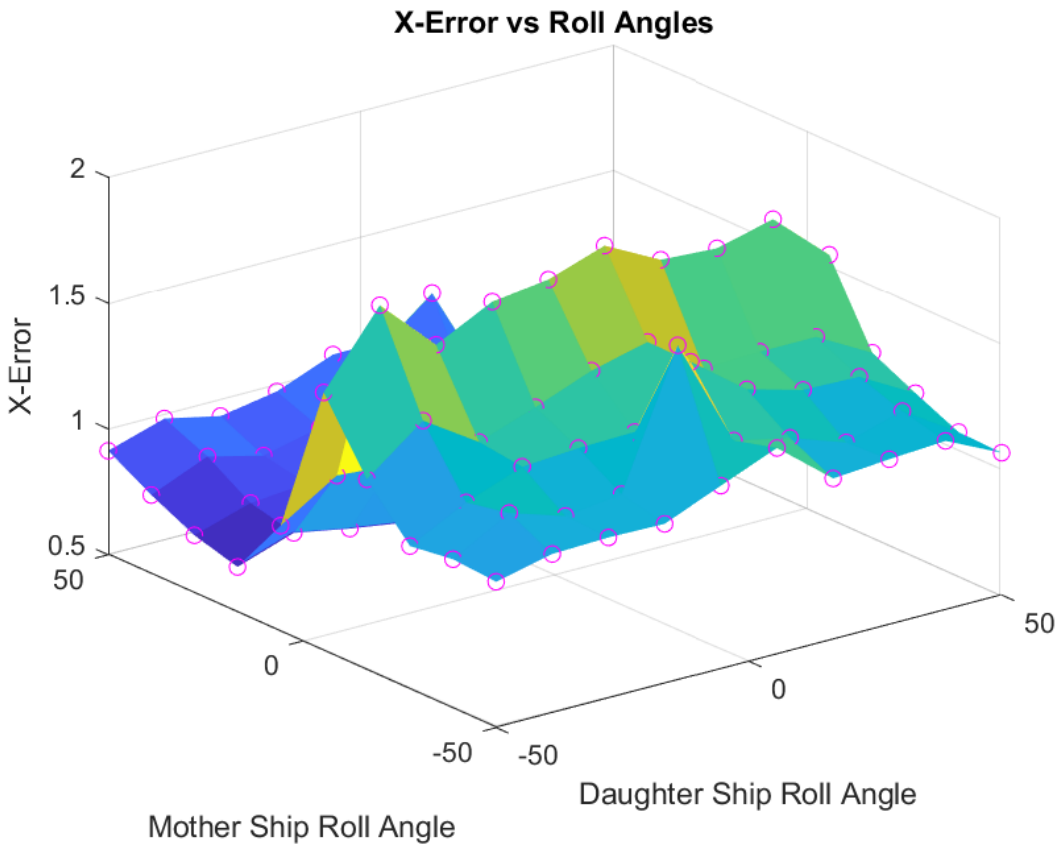


Figure 12: Surface plot comparing ship velocities to X-error. The magnitudes of the error remain low, but clearly rise as Ship 2 approaches zero degrees of roll angle.

is especially prominent in the X-error plot. Similar spikes, yet not as apparent, show themselves in the Y-error plot.

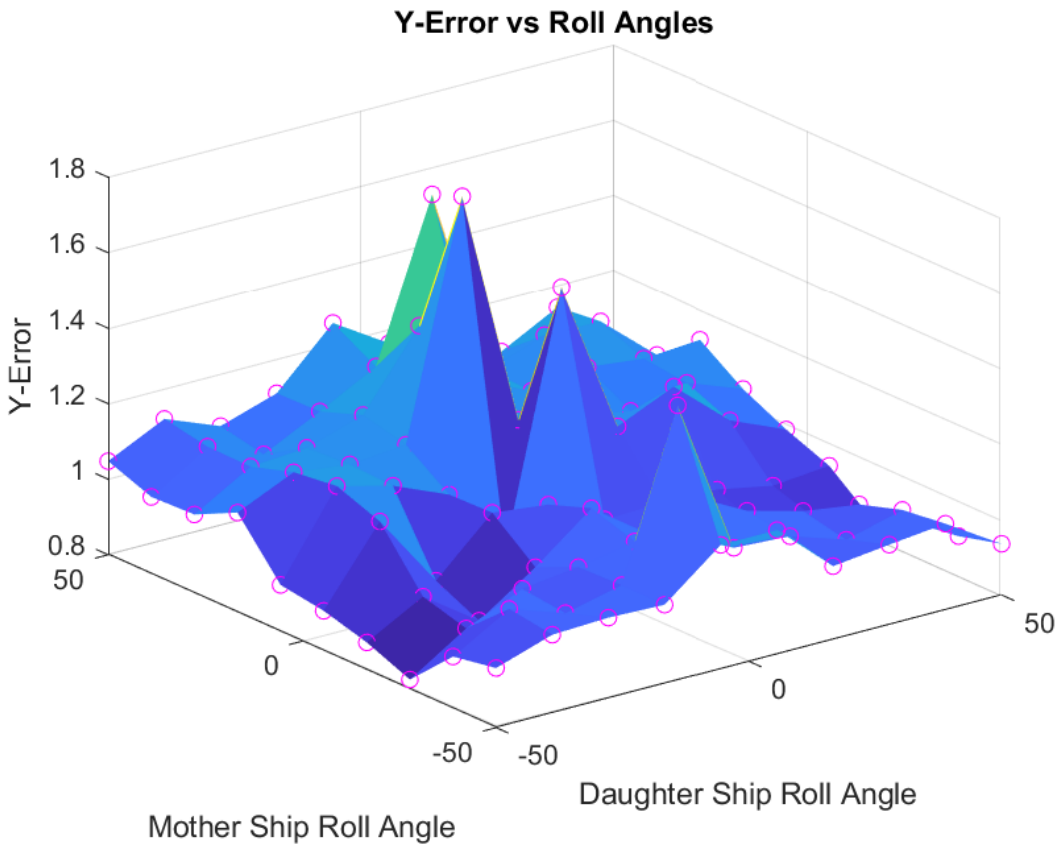


Figure 13: Surface plot comparing ship velocities to X-error. The magnitudes of the error are low, but less cohesive than the X-error plot. Slightly higher error values can be observed closer to the zero degree line.

### 4.5 Effect of Varied Altitude Values

Altitude has little impact on the error between the truth and predicted values of Ship 2. The tested values of Ship 1 altitudes ranged from 100 meters to 10,000 meters and the values of Ship 2 ranged from 50 meters to 3,000 meters. The numerical results of the altitude experiments are shown in Table 8. The error values are tightly distributed within a range between 1 and 2 meters. Note that the error values are the maximum, minimum, and average error results obtained from a 50-run average. Figure 14 and Figure 15 show surface plots of the altitude experiment tests, plotting Ship 1, Ship 2, and X and Y error, respectively.

Table 8: Altitude Simulation Results, 50-Run Average

| **Description** | **Value** |
|---|---|
| Minimum X Error | 0.983 m |
| Maximum X Error | 1.278 m |
| Average X Error | 1.114 m |
| Minimum Y Error | 1.192 m |
| Maximum Y Error | 1.461 m |
| Average Y Error | 1.313 m |
| Minimum Total Error | 1.516 m |
| Maximum Total Error | 1.941 m |
| Average Total Error | 1.722 m |

It can be observed that the error is generally lower as the two ships become closer in altitude. The error is lowest as the ships are co-altitude. The altitude of Ship 2 seems to have a larger effect on the total error, however the magnitude of the error is small.


Figure 14: Surface plot comparing ship altitudes to X-error. The magnitude of the error is low across the range of tested values.

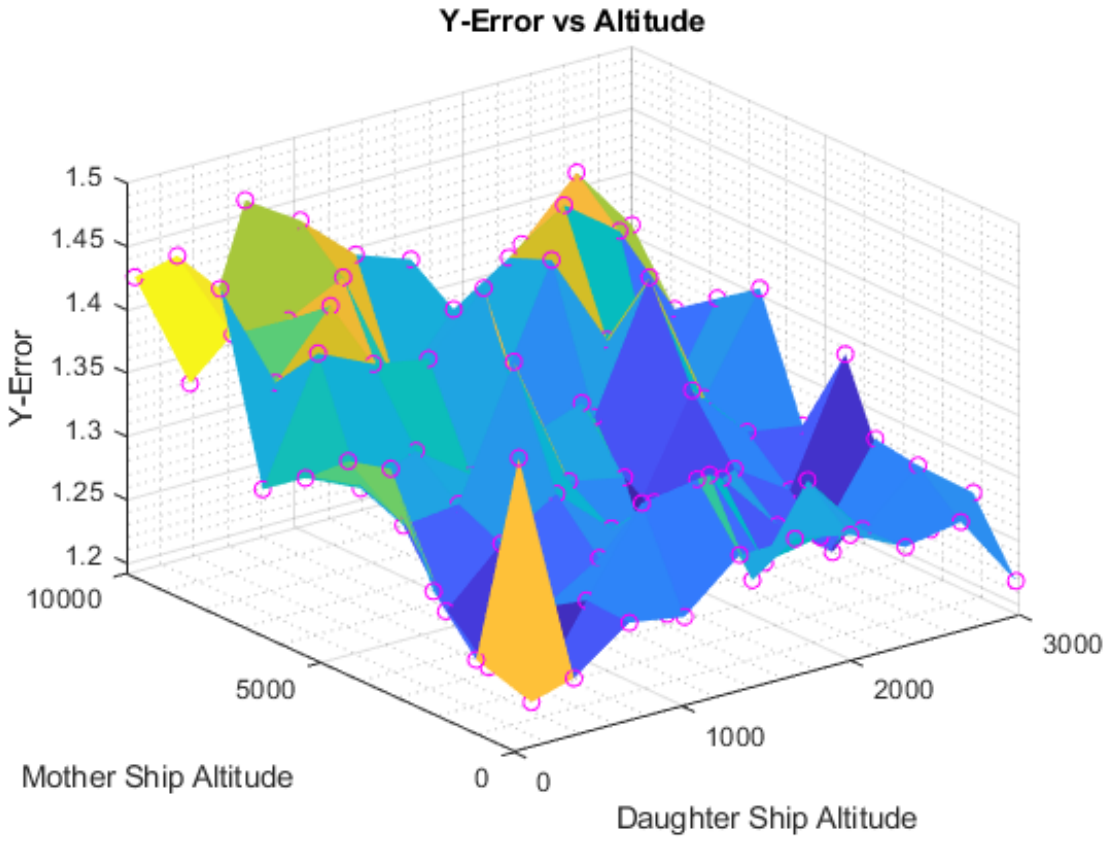


Figure 15: Surface plot comparing ship altitudes to Y-error. The magnitude of the error is low across the range of tested values.

### 4.6 Effects of Varied Separation Distance Values

Separation distance has little to no impact on the error between the truth and predicted values of Ship 2. The tested values of the separation distance ranged from 500 meters to 100,000 meters. The numerical values of the separation distance experiments are shown in Table 9. Note that the error values are the maximum, minimum, and average error results obtained from a 50-run average. Figure 16 and Figure 17 show separation distance plotted against X and Y error, respectively. Figure 18 shows the separation distance plotted against the average total error.

Table 9: Separation Distance Simulation Results, 50-Run Average

| **Description** | **Value** |
|---|---|
| Minimum X Error | 0.876 m |
| Maximum X Error | 0.949 m |
| Average X Error | 0.919 m |
| Minimum Y Error | 1.104 m |
| Maximum Y Error | 1.213 m |
| Average Y Error | 1.176 m |
| Minimum Total Error | 1.409 m |
| Maximum Total Error | 1.532 m |
| Average Total Error | 1.492 m |

Error generally remains below 1 meter in the X direction and between 1.15 and 1.30 meters in the Y direction. The small magnitude of the error could simply be noise in the data. It should be noted that one of the primary assumptions of the experiment is that the ranging link between the two ships remains intact. This assumption negates some of the reasoning behind testing separation distance. Factors such as atmospheric interference can effect the behavior of the ranging link in the real world. These factors are not accounted for in the separation distance testing. Noise in the ranging sensor is examined later in this chapter.

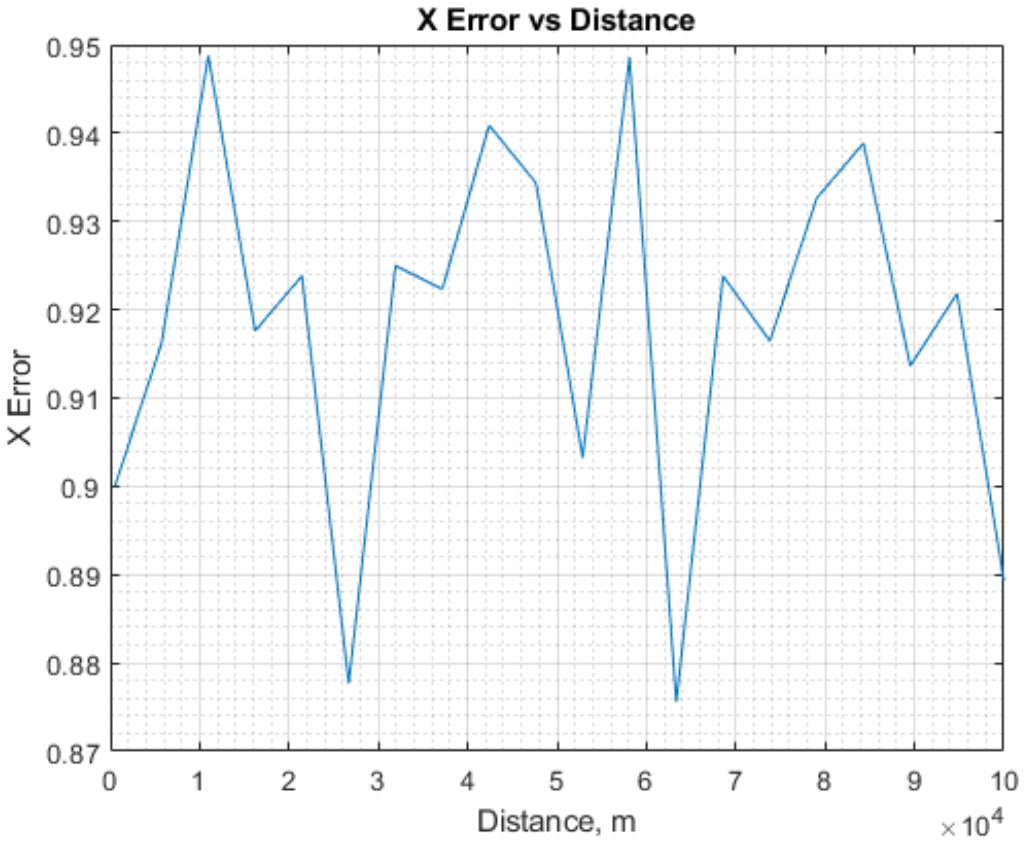


Figure 16: Plot comparing separation distance to X-error. Separation distance has little to no impact on the error. The magnitude of the error is very small and could be accounted for by noise.

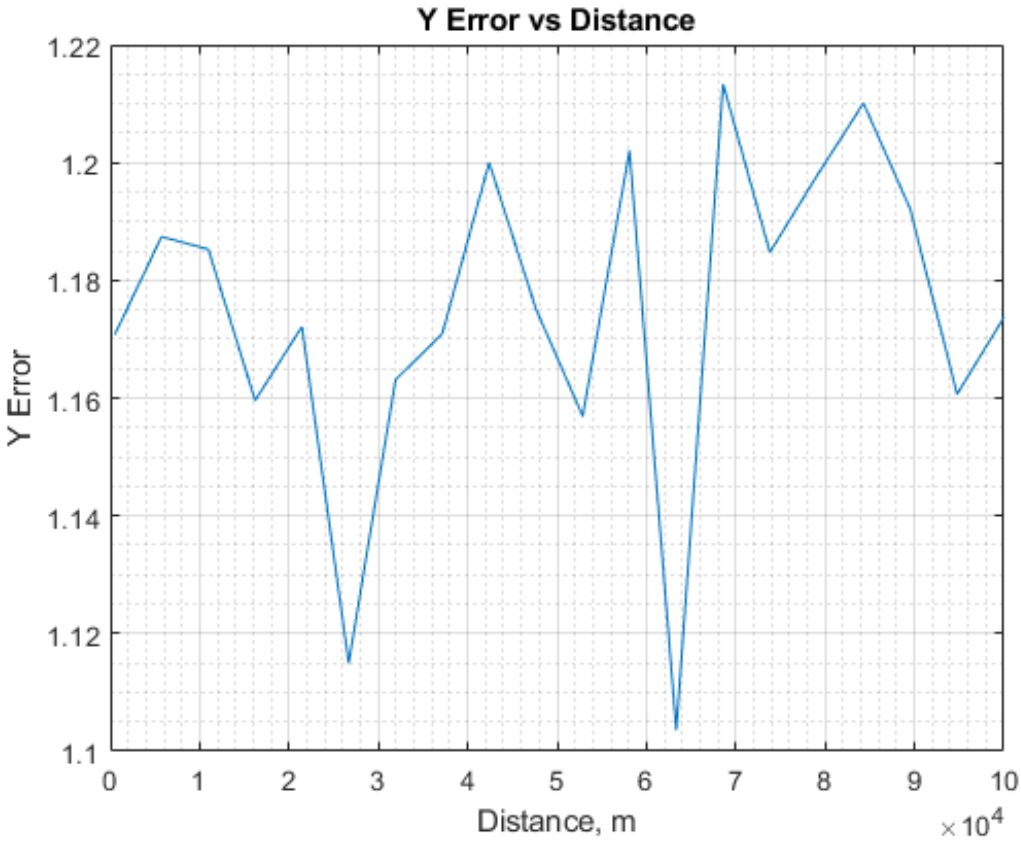


Figure 17: Plot comparing separation distance to Y-error. Separation distance has little to no impact on the error. The magnitude of the error is very small and could be accounted for by noise.

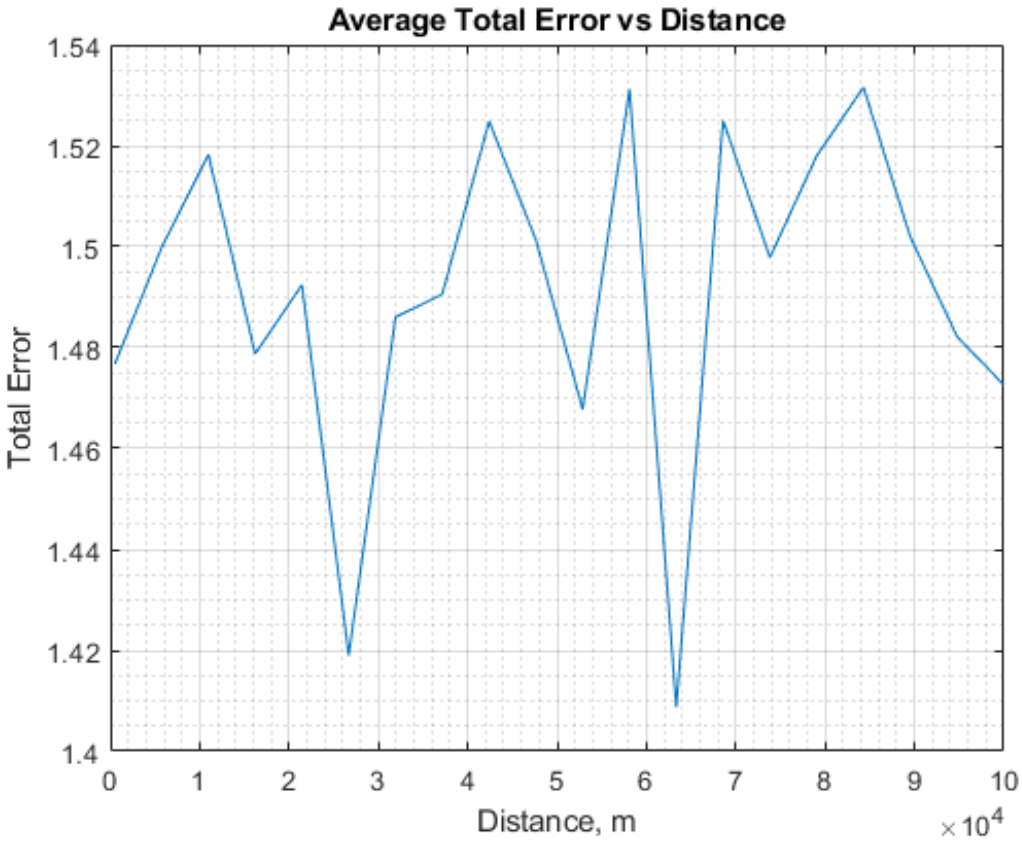


Figure 18: Plot comparing separation distance to the average total error. Separation distance has little to no impact on the error. The magnitude of the error is very small and could be accounted for by noise.

### 4.7 Effects of Varied Range Sensor Noise Values

Range sensor noise has a noticeable impact on the error between the truth and predicted values of Ship 2. The tested values of the range sensor noise were from $0.001^2$ to $2^2$. Table 10 shows the numerical results of the range sensor noise experiments. Note that the error values are the maximum, minimum, and average error results obtained from a 50-run average. Figure 19 and Figure 20 show range sensor noise plotted against X and Y error, respectively. Figure 21 shows the range sensor noise plotted against the average total error. It should be noted that this is a squared value in the simulation, therefore all numbers shown have had the square root of the raw data taken in order to make the data more presentable.

Table 10: Range Sensor Noise Simulation Results, 50-Run Average

| **Description** | **Value** |
|---|---|
| Minimum X Error | 0.370 m |
| Maximum X Error | 2.057 m |
| Average X Error | 1.718 m |
| Minimum Y Error | 0.419 m |
| Maximum Y Error | 2.336 m |
| Average Y Error | 1.962 m |
| Minimum Total Error | 0.559 m |
| Maximum Total Error | 3.113 m |
| Average Total Error | 2.608 m |

As the sensor noise value increases, the error present between the predicted and actual values of Ship 2 increases. The error increases linearly until about 0.45 on the range sensor noise scale and then begins to climb more slowly. This behavior is exhibited in both X and Y. The error continues to rise as the range sensor noise value increases. The testing range stops at 2 but the same behavior continues outside of the tested range. Note that most current manufacturers of ranging devices claim centimeter or better accuracy levels, making even large range errors pessimistic.

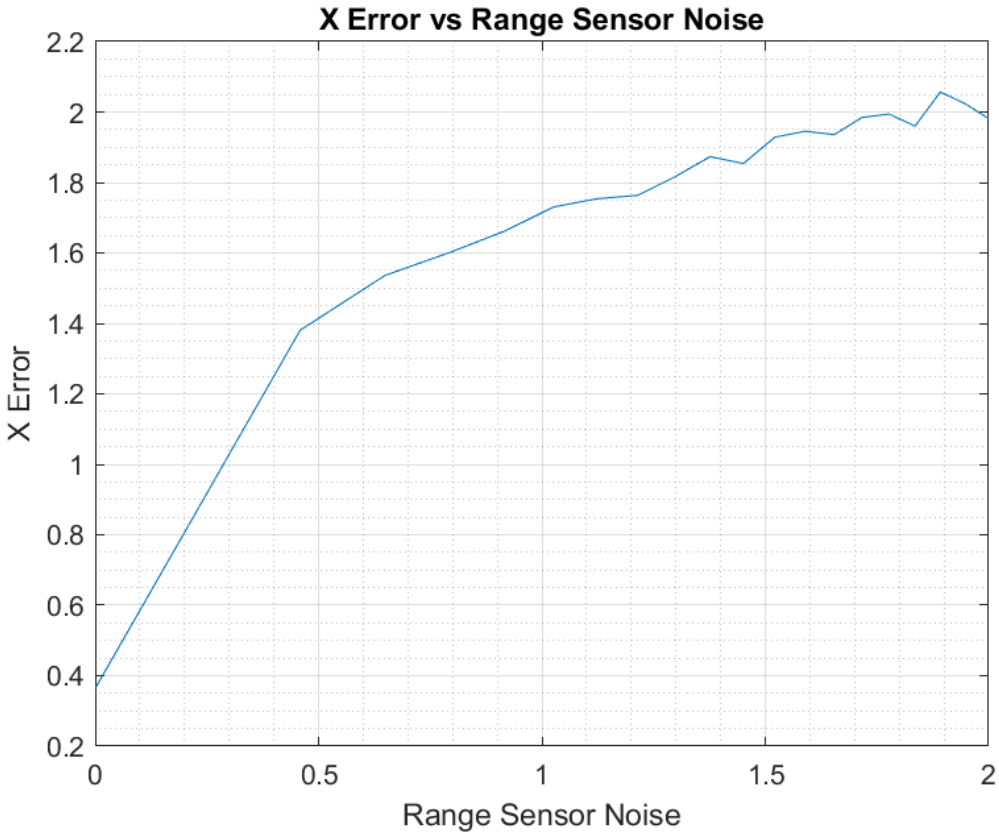


Figure 19: Plot comparing range sensor noise to X-error. The noise has a noticeable impact on error and should be kept as low as possible for best performance.

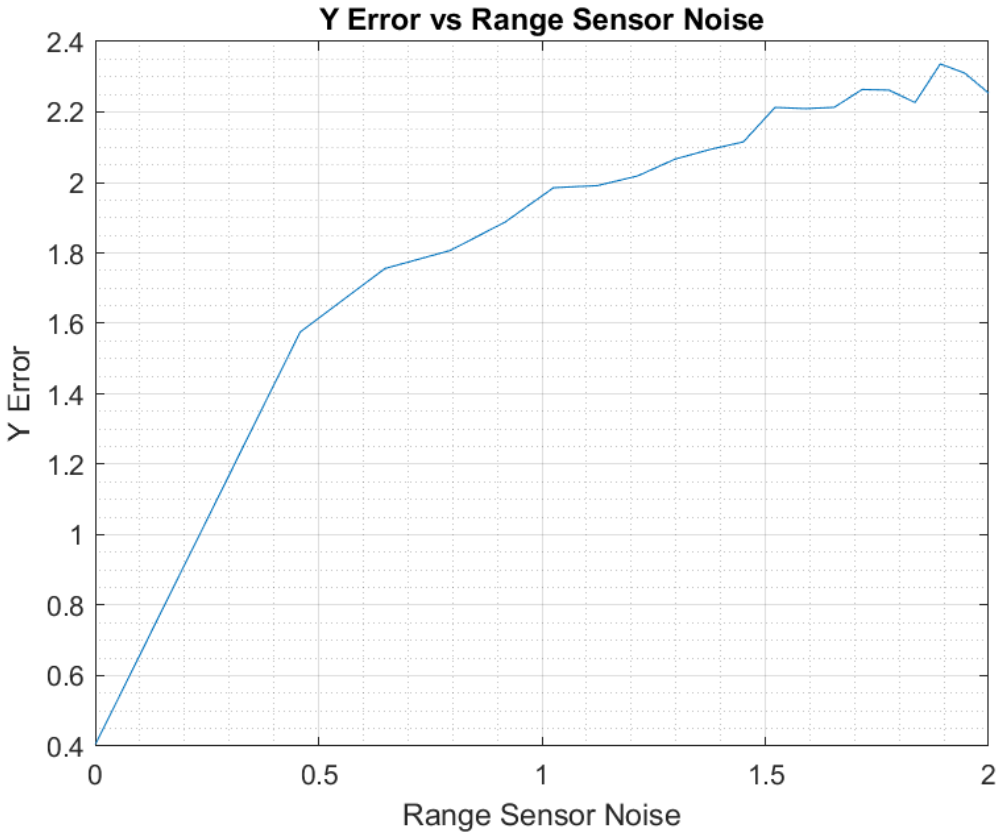


Figure 20: Plot comparing range sensor noise to Y-error. The noise has a noticeable impact on error and should be kept as low as possible for best performance.

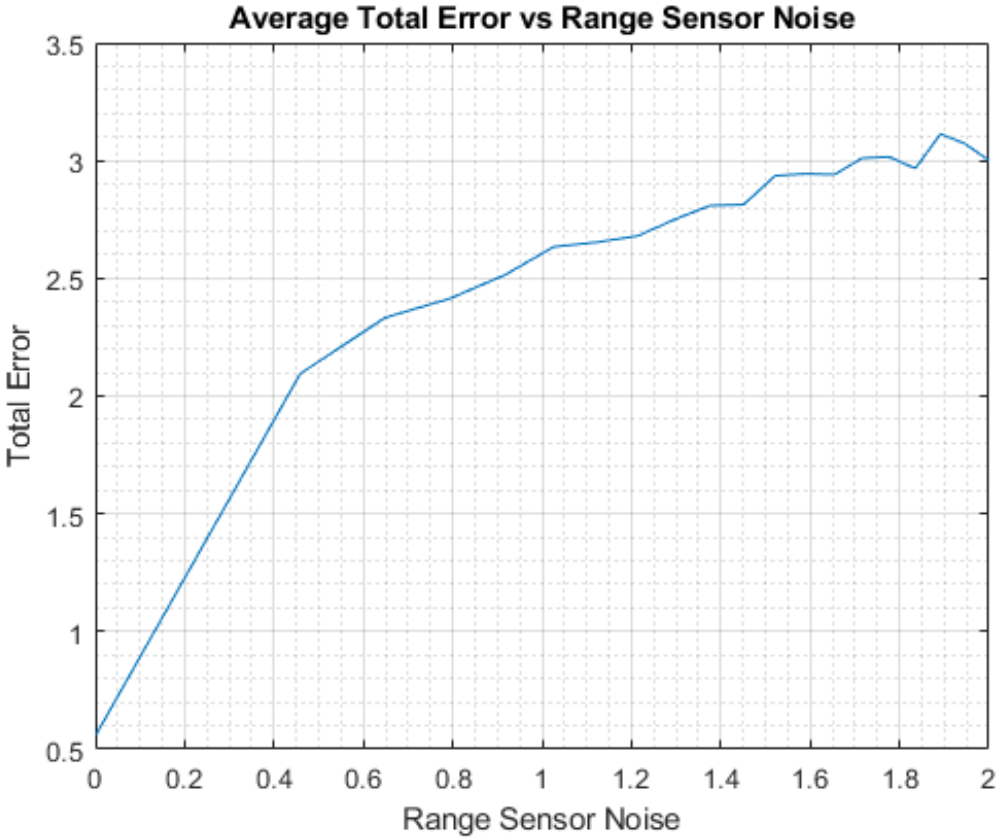


Figure 21: Plot comparing range sensor noise to average total error. The noise has a noticeable impact on error and should be kept as low as possible for best performance.

### 4.8 Effects of Varied Ship 2 IMU Uncertainty Values

The uncertainty of the IMU has a noticeable impact on the error between the truth and predicted values of Ship 2. The tested values of the IMU uncertainty were from $0.00001^2$ to $0.02^2$. Table 11 shows the numerical results of the IMU uncertainty experiments. Note that the error values are the maximum, minimum, and average error results obtained from a 50-run average. Figure 22 and Figure 23 show IMU uncertainty plotted against X and Y error, respectively. Figure 24 shows the IMU uncertainty plotted against the average total error. It should be noted that this is a squared value in the simulation, therefore all numbers shown have had the square root of the raw data taken in order to make the data more presentable.

Table 11: IMU Uncertainty Simulation Results, 50-Run Average

| **Description** | **Value** |
|---|---|
| Minimum X Error | 0.167 m |
| Maximum X Error | 1.312 m |
| Average X Error | 1.067 m |
| Minimum Y Error | 0.182 m |
| Maximum Y Error | 1.479 m |
| Average Y Error | 1.213 m |
| Minimum Total Error | 0.247 m |
| Maximum Total Error | 1.977 m |
| Average Total Error | 1.615 m |

Very small changes to the IMU uncertainty of Ship 2 result in large increases in error. Similar to the behavior exhibited by the range sensor noise, the IMU uncertainty increases linearly until about 0.006 at which time it begins a slower increase. Of note however, is the range of values of which the tests are run. As seen in Table 3, the IMU uncertainty of Ship 2 is tested over a range from $0.00001^2$ to $0.02^2$. The uncertainty of the IMU of Ship 2 cannot be much larger than the maximum tested value, as doing so makes the error rise sharply. This is expected behavior, as increasing the uncertainty

of the IMU of Ship 2 decreases the confidence of the filter which allows it to diverge. For best performance, it is recommended to keep IMU uncertainty low by utilizing a good quality IMU.

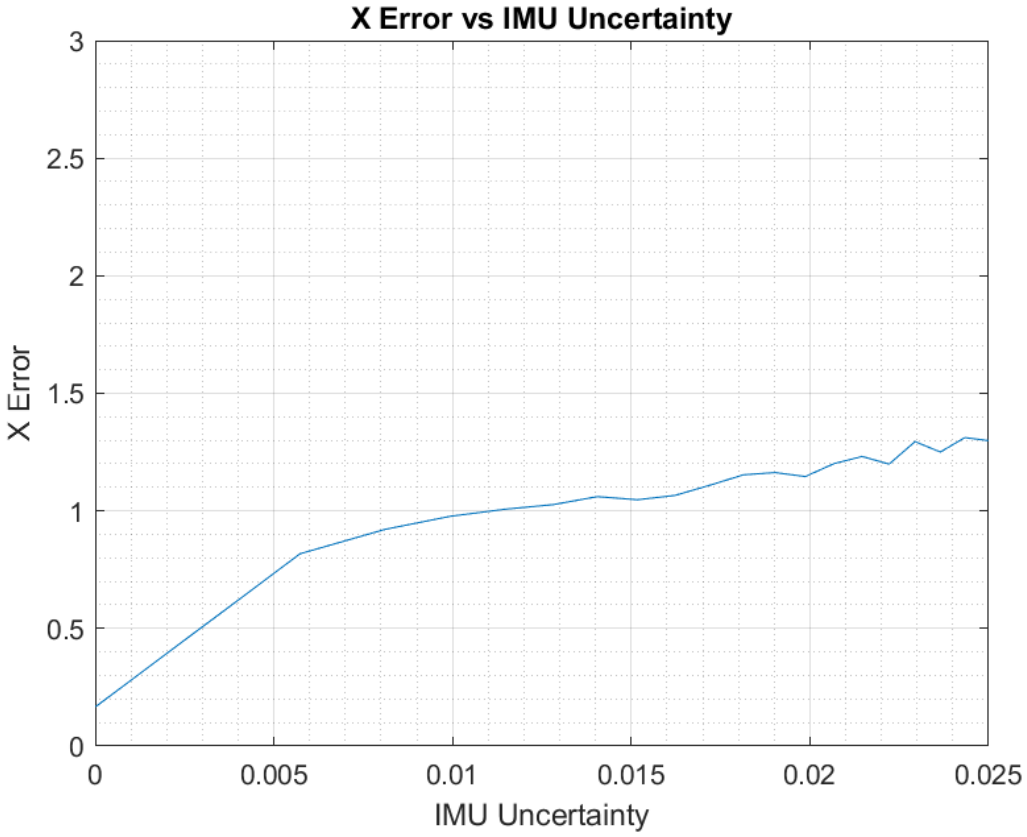


Figure 22: Plot comparing the Ship 2 IMU uncertainty to X-error. The uncertainty has a noticeable impact on error. The error rises sharply outside of the tested range rendering the filter unstable.

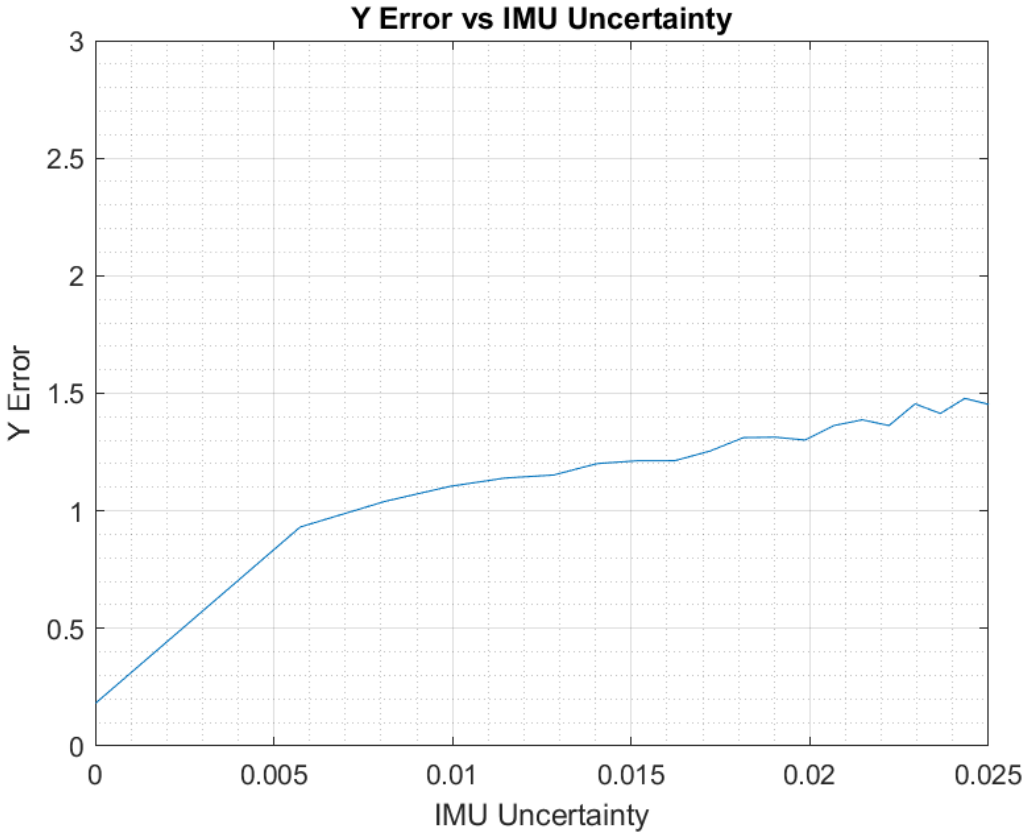


Figure 23: Plot comparing the Ship 2 IMU uncertainty to Y-error. The uncertainty has a noticeable impact on error. The error rises sharply outside of the tested range rendering the filter unstable.

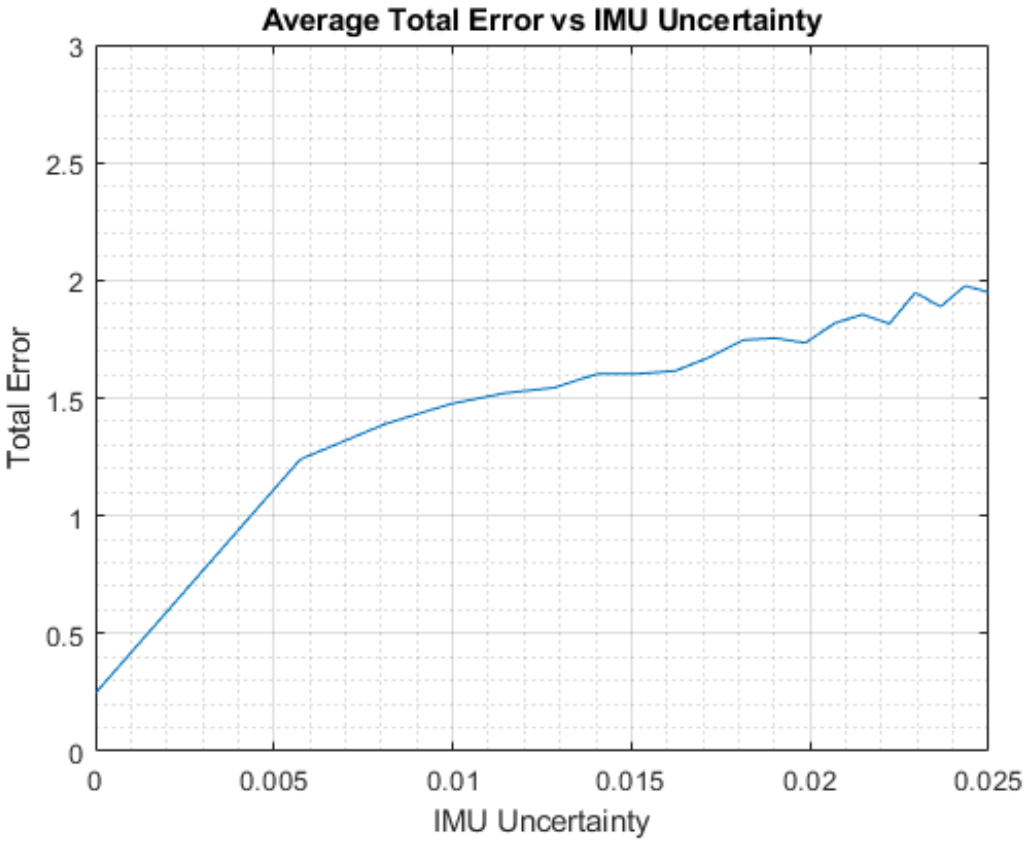


Figure 24: Plot comparing the Ship 2 IMU uncertainty to the average total error. The uncertainty has a noticeable impact on error. The error rises sharply outside of the tested range rendering the filter unstable.

## 4.9 Acceptable Parameters

In order to draw useful conclusions about the range of parameters in which this approach is viable, a benchmark value of 3 meters of error was set. The value of 3 meters of error was chosen to allow for use in operational environments to be accurate under GPS-denied conditions and falls below the civilian GPS average error of 5 meters. Table 12 gives the test range and unacceptable conditions for the tested parameters.

Table 12: Test Range and Unacceptable Conditions

| **Parameter** | **Test Range** | **Unacceptable Conditions** |
|---|---|---|
| Velocity, Ship 1 | 75 m/s - 150 m/s | None |
| Velocity, Ship 2 | 5 m/s - 30 m/s | Above 25 m/s |
| Roll Angle, Ship 1 | -50° - 50° | 0° |
| Roll Angle, Ship 2 | -50° - 50° | 0° |
| Altitude, Ship 1 | 100 m - 10,000 m | None |
| Altitude, Ship 2 | 50 m - 3,000 m | None |
| Separation Distance | 500 m - 100,000 m | None |
| Range Sensor Noise | $0.001^2$ - $2^2$ | Above $0.1^2$ |
| IMU Uncertainty, Ship 2 | $0.00001^2$ - $0.02^2$ | Above $0.01^2$ |

# V. Conclusions

## 5.1 Overview

This section summarizes the research and results of the work performed during the experimental tests. Section 5.2 reiterates the notable conclusions found by the testing and analysis of the simulation. Section 5.3 provides possibilities for future work in line with the planned execution of this research.

## 5.2 Research Conclusions

This research was successful in meeting the objectives it set out to accomplish: first, to establish that the approach of using only the ranging link between the mothership and daughter-ship to achieve a position solution is viable; second, to examine the impact that various parameters have on the performance of the position solution; and third, to establish the range of parameters at which the daughter-ship can operate in successfully.

As hypothesized, the GPS-denied daughter-ship is able to be located by using just measurements from the ranging link between the mother and daughter-ship. The amount of total error between the measured location of the daughter-ship and the predicted location from utilizing the ranging link is about 2 meters. The approach, therefore, is deemed viable by the results of the simulation.

Additional conclusions can be drawn from the work when analyzing the effect that flight parameters have on the accuracy of the position solution. The velocity of the two ships moderately impacts the accuracy of the position solution and the daughter-ship should remain under 25 meters per second to minimize error. Roll angle has little impact on the accuracy of the position solution, however both ships should avoid a roll angle of zero degrees as this does not allow the filter to operate

properly. Altitude also has little impact on the accuracy of the position solution with the accuracy tending to increase as the ships become closer in altitude, the greatest accuracy being when the ships are co-altitude. Separation distance has little to no impact on the accuracy of the position solution and is tested with the assumption that the ranging link remains intact for the duration of the flight. Therefore, impacts on error are minimized. Range sensor noise has a large impact on the position solution with the position solution rapidly failing outside of the tested range. As expected, adding noise to the range sensor quickly degrades the usefulness of the solution. Daughter-ship IMU uncertainty also has a noticeable impact on the position solution. Again, the solution rapidly degrades outside of the tested range and quickly makes the filter fail. Accordingly, the IMU used in this solution should be of high quality in order to keep the error at a minimum.

## 5.3 Future Work

Future work should focus on a few key areas. First, this research assumed a ranging radio exists that can achieve the desired performance specifications. Work should be accomplished to locate or design such a radio that is capable of performing the experiments laid out in this research. Additionally, a look can be taken at some of the other assumptions such as timing synchronicity and atmospheric impacts. The simulation could also be expanded to handle additional parameters or ships operating cooperatively as well as making the operation more user friendly and able to plot the ships trajectory real-time. Finally, the approach should be tested in the real world on hardware in a low-cost, original system before being flight tested on the desired hardware.

# Appendix A. Full Simulation Results

Table 13: Velocity Tests, Full Results

| Sim Name | Description | | X-Error | Y-Error | Total Error |
|---|---|---|---|---|---|
| Baseline | V1=125, V2=15 | | 0.936 | 1.193 | 1.516359 |
| V_1_1 | 75 | 5 | 0.771181 | 0.868191 | 1.161239 |
| V_1_2 | 75 | 7.777778 | 0.935092 | 1.042325 | 1.400299 |
| V_1_3 | 75 | 10.55556 | 1.103391 | 1.229607 | 1.652091 |
| V_1_4 | 75 | 13.33333 | 1.347196 | 1.478373 | 2.000131 |
| V_1_5 | 75 | 16.11111 | 1.477591 | 1.597713 | 2.176226 |
| V_1_6 | 75 | 18.88889 | 1.54198 | 1.670803 | 2.273607 |
| V_1_7 | 75 | 21.66667 | 1.914747 | 2.007275 | 2.77406 |
| V_1_8 | 75 | 24.44444 | 2.364593 | 2.471868 | 3.420735 |
| V_1_9 | 75 | 27.22222 | 3.825553 | 3.97118 | 5.514084 |
| V_1_10 | 75 | 30 | 3.209552 | 3.251453 | 4.568716 |
| V_2_1 | 83.33333 | 5 | 0.699807 | 0.807453 | 1.068508 |
| V_2_2 | 83.33333 | 7.777778 | 0.890878 | 1.028235 | 1.360489 |
| V_2_3 | 83.33333 | 10.55556 | 1.019634 | 1.163427 | 1.547002 |
| V_2_4 | 83.33333 | 13.33333 | 1.186078 | 1.332302 | 1.783763 |
| V_2_5 | 83.33333 | 16.11111 | 1.464462 | 1.616376 | 2.181128 |
| V_2_6 | 83.33333 | 18.88889 | 1.501876 | 1.627426 | 2.214531 |

Continued on next page

**Table 13 – continued from previous page**

| Sim Name | Description | | X-Error | Y-Error | Total Error |
|---|---|---|---|---|---|
| V_2_7 | 83.33333 | 21.66667 | 1.706091 | 1.840369 | 2.509523 |
| V_2_8 | 83.33333 | 24.44444 | 2.068871 | 2.198267 | 3.018709 |
| V_2_9 | 83.33333 | 27.22222 | 2.522446 | 2.639283 | 3.650828 |
| V_2_10 | 83.33333 | 30 | 4.229751 | 4.418677 | 6.116821 |
| V_3_1 | 91.66667 | 5 | 0.666879 | 0.783991 | 1.029257 |
| V_3_2 | 91.66667 | 7.777778 | 0.817181 | 0.987831 | 1.282028 |
| V_3_3 | 91.66667 | 10.55556 | 0.960342 | 1.101509 | 1.461362 |
| V_3_4 | 91.66667 | 13.33333 | 1.061135 | 1.255018 | 1.643496 |
| V_3_5 | 91.66667 | 16.11111 | 1.271317 | 1.473612 | 1.946222 |
| V_3_6 | 91.66667 | 18.88889 | 1.518411 | 1.715036 | 2.290616 |
| V_3_7 | 91.66667 | 21.66667 | 1.621891 | 1.781791 | 2.409421 |
| V_3_8 | 91.66667 | 24.44444 | 1.963423 | 2.102898 | 2.877014 |
| V_3_9 | 91.66667 | 27.22222 | 2.35192 | 2.522894 | 3.449134 |
| V_3_10 | 91.66667 | 30 | 3.572615 | 3.686165 | 5.133361 |
| V_4_1 | 100 | 5 | 0.597302 | 0.753579 | 0.961588 |
| V_4_2 | 100 | 7.777778 | 0.748649 | 0.918849 | 1.185225 |
| V_4_3 | 100 | 10.55556 | 0.908114 | 1.122867 | 1.444127 |
| V_4_4 | 100 | 13.33333 | 1.009486 | 1.208098 | 1.574345 |

Continued on next page

**Table 13 – continued from previous page**

| Sim Name | Description | | X-Error | Y-Error | Total Error |
|---|---|---|---|---|---|
| V_4_5 | 100 | 16.11111 | 1.209775 | 1.410386 | 1.858156 |
| V_4_6 | 100 | 18.88889 | 1.738402 | 2.074979 | 2.706951 |
| V_4_7 | 100 | 21.66667 | 1.588192 | 1.766964 | 2.375819 |
| V_4_8 | 100 | 24.44444 | 1.875887 | 2.055558 | 2.782853 |
| V_4_9 | 100 | 27.22222 | 2.372979 | 2.538003 | 3.474548 |
| V_4_10 | 100 | 30 | 3.138722 | 3.234435 | 4.507011 |
| V_5_1 | 108.3333 | 5 | 0.557213 | 0.721819 | 0.911871 |
| V_5_2 | 108.3333 | 7.777778 | 0.697003 | 0.881953 | 1.124124 |
| V_5_3 | 108.3333 | 10.55556 | 0.832743 | 1.03949 | 1.331916 |
| V_5_4 | 108.3333 | 13.33333 | 1.003111 | 1.186049 | 1.553365 |
| V_5_5 | 108.3333 | 16.11111 | 1.126741 | 1.371893 | 1.775285 |
| V_5_6 | 108.3333 | 18.88889 | 1.347279 | 1.608586 | 2.098264 |
| V_5_7 | 108.3333 | 21.66667 | 1.573709 | 1.843741 | 2.424034 |
| V_5_8 | 108.3333 | 24.44444 | 1.725187 | 1.979989 | 2.626143 |
| V_5_9 | 108.3333 | 27.22222 | 2.253161 | 2.486609 | 3.355587 |
| V_5_10 | 108.3333 | 30 | 3.081274 | 3.291837 | 4.508929 |
| V_6_1 | 116.6667 | 5 | 0.524134 | 0.678942 | 0.857717 |
| V_6_2 | 116.6667 | 7.777778 | 0.654183 | 0.85481 | 1.076408 |

Continued on next page

**Table 13 – continued from previous page**

| Sim Name | Description | | X-Error | Y-Error | Total Error |
|---|---|---|---|---|---|
| V_6_3 | 116.6667 | 10.55556 | 0.796567 | 1.042828 | 1.312253 |
| V_6_4 | 116.6667 | 13.33333 | 0.903318 | 1.139399 | 1.454034 |
| V_6_5 | 116.6667 | 16.11111 | 1.086866 | 1.341899 | 1.726838 |
| V_6_6 | 116.6667 | 18.88889 | 1.320303 | 1.578478 | 2.057861 |
| V_6_7 | 116.6667 | 21.66667 | 1.77805 | 2.165219 | 2.80172 |
| V_6_8 | 116.6667 | 24.44444 | 1.909691 | 2.114377 | 2.849124 |
| V_6_9 | 116.6667 | 27.22222 | 2.251648 | 2.420525 | 3.305882 |
| V_6_10 | 116.6667 | 30 | 2.646517 | 2.837651 | 3.880247 |
| V_7_1 | 125 | 5 | 0.511669 | 0.669076 | 0.8423 |
| V_7_2 | 125 | 7.777778 | 0.61241 | 0.81976 | 1.023256 |
| V_7_3 | 125 | 10.55556 | 0.725835 | 0.947319 | 1.19342 |
| V_7_4 | 125 | 13.33333 | 0.856291 | 1.124992 | 1.413804 |
| V_7_5 | 125 | 16.11111 | 1.042415 | 1.31227 | 1.675912 |
| V_7_6 | 125 | 18.88889 | 1.200706 | 1.512123 | 1.930857 |
| V_7_7 | 125 | 21.66667 | 1.48988 | 1.83131 | 2.360813 |
| V_7_8 | 125 | 24.44444 | 1.819555 | 2.001132 | 2.704683 |
| V_7_9 | 125 | 27.22222 | 2.143794 | 2.362493 | 3.190177 |
| V_7_10 | 125 | 30 | 2.63749 | 2.823937 | 3.864062 |

Continued on next page

**Table 13 – continued from previous page**

| Sim Name | Description | | X-Error | Y-Error | Total Error |
|---|---|---|---|---|---|
| V_8_1 | 133.3333 | 5 | 0.476359 | 0.654427 | 0.809439 |
| V_8_2 | 133.3333 | 7.777778 | 0.59378 | 0.809573 | 1.003984 |
| V_8_3 | 133.3333 | 10.55556 | 0.730158 | 0.939865 | 1.190158 |
| V_8_4 | 133.3333 | 13.33333 | 0.848186 | 1.088397 | 1.379865 |
| V_8_5 | 133.3333 | 16.11111 | 1.005222 | 1.278765 | 1.626565 |
| V_8_6 | 133.3333 | 18.88889 | 1.193945 | 1.552703 | 1.958671 |
| V_8_7 | 133.3333 | 21.66667 | 1.495877 | 1.810883 | 2.348818 |
| V_8_8 | 133.3333 | 24.44444 | 1.945907 | 2.253071 | 2.97706 |
| V_8_9 | 133.3333 | 27.22222 | 2.361192 | 2.558409 | 3.481478 |
| V_8_10 | 133.3333 | 30 | 2.894131 | 3.089239 | 4.23313 |
| V_9_1 | 141.6667 | 5 | 0.446976 | 0.626999 | 0.77001 |
| V_9_2 | 141.6667 | 7.777778 | 0.563615 | 0.778171 | 0.960839 |
| V_9_3 | 141.6667 | 10.55556 | 0.680064 | 0.967066 | 1.182245 |
| V_9_4 | 141.6667 | 13.33333 | 0.829823 | 1.100146 | 1.378016 |
| V_9_5 | 141.6667 | 16.11111 | 0.968074 | 1.25136 | 1.582109 |
| V_9_6 | 141.6667 | 18.88889 | 1.217321 | 1.497084 | 1.929542 |
| V_9_7 | 141.6667 | 21.66667 | 1.506443 | 1.769145 | 2.323628 |
| V_9_8 | 141.6667 | 24.44444 | 1.851141 | 2.119076 | 2.813753 |

Continued on next page

**Table 13 – continued from previous page**

| Sim Name | Description | | X-Error | Y-Error | Total Error |
|---|---|---|---|---|---|
| V_9_9 | 141.6667 | 27.22222 | 2.417736 | 2.643364 | 3.582293 |
| V_9_10 | 141.6667 | 30 | 2.896336 | 3.110373 | 4.25008 |
| V_10_1 | 150 | 5 | 0.435662 | 0.603868 | 0.744619 |
| V_10_2 | 150 | 7.777778 | 0.538383 | 0.773902 | 0.942751 |
| V_10_3 | 150 | 10.55556 | 0.643494 | 0.903275 | 1.10905 |
| V_10_4 | 150 | 13.33333 | 0.796746 | 1.047922 | 1.316413 |
| V_10_5 | 150 | 16.11111 | 0.935285 | 1.23017 | 1.54534 |
| V_10_6 | 150 | 18.88889 | 1.212555 | 1.502069 | 1.930415 |
| V_10_7 | 150 | 21.66667 | 1.589588 | 1.802178 | 2.403048 |
| V_10_8 | 150 | 24.44444 | 2.030492 | 2.239674 | 3.023084 |
| V_10_9 | 150 | 27.22222 | 2.545509 | 2.773897 | 3.764854 |
| V_10_10 | 150 | 30 | 3.257892 | 3.300411 | 4.637518 |

Table 14: Roll Angle Tests, Full Results

| Sim Name | Description | | X-Error | Y-Error | Total Error |
|---|---|---|---|---|---|
| Baseline | RA1=0.4363, RA2=0.0873 | | 0.936 | 1.193 | 1.516359 |
| RA_1_1 | -0.8727 | -0.8727 | 1.089224 | 0.964884 | 1.455132 |

Continued on next page

**Table 14 – continued from previous page**

| Sim Name | Description | | X-Error | Y-Error | Total Error |
|---|---|---|---|---|---|
| RA_1_2 | -0.8727 | -0.6788 | 1.254147 | 1.116561 | 1.679164 |
| RA_1_3 | -0.8727 | -0.4848 | 1.206916 | 1.064268 | 1.609135 |
| RA_1_4 | -0.8727 | -0.2909 | 1.203112 | 1.068407 | 1.609028 |
| RA_1_5 | -0.8727 | -0.0970 | 1.248746 | 1.13963 | 1.690599 |
| RA_1_6 | -0.8727 | 0.0970 | 1.32861 | 1.132895 | 1.74604 |
| RA_1_7 | -0.8727 | 0.2909 | 1.255481 | 1.098238 | 1.668041 |
| RA_1_8 | -0.8727 | 0.4848 | 1.218963 | 1.073086 | 1.624002 |
| RA_1_9 | -0.8727 | 0.6788 | 1.251582 | 1.097994 | 1.664947 |
| RA_1_10 | -0.8727 | 0.8727 | 1.149005 | 1.004698 | 1.526313 |
| RA_2_1 | -0.6788 | -0.8727 | 1.178126 | 0.996956 | 1.543341 |
| RA_2_2 | -0.6788 | -0.6788 | 1.224043 | 1.061451 | 1.620173 |
| RA_2_3 | -0.6788 | -0.4848 | 1.226843 | 1.03126 | 1.602698 |
| RA_2_4 | -0.6788 | -0.2909 | 1.27834 | 1.078873 | 1.672758 |
| RA_2_5 | -0.6788 | -0.0970 | 1.594503 | 1.373095 | 2.104241 |
| RA_2_6 | -0.6788 | 0.0970 | 1.497656 | 1.17563 | 1.903964 |
| RA_2_7 | -0.6788 | 0.2909 | 1.282302 | 1.082477 | 1.67811 |
| RA_2_8 | -0.6788 | 0.4848 | 1.289306 | 1.049976 | 1.662756 |
| RA_2_9 | -0.6788 | 0.6788 | 1.270062 | 1.079144 | 1.666616 |

Continued on next page

**Table 14 – continued from previous page**

| Sim Name | Description | | X-Error | Y-Error | Total Error |
|---|---|---|---|---|---|
| RA_2_10 | -0.6788 | 0.8727 | 1.183809 | 1.000419 | 1.549916 |
| RA_3_1 | -0.4848 | -0.8727 | 1.20931 | 0.966119 | 1.547842 |
| RA_3_2 | -0.4848 | -0.6788 | 1.319085 | 1.057277 | 1.690509 |
| RA_3_3 | -0.4848 | -0.4848 | 1.33413 | 1.05958 | 1.703705 |
| RA_3_4 | -0.4848 | -0.2909 | 1.300199 | 1.034633 | 1.661621 |
| RA_3_5 | -0.4848 | -0.0970 | 1.3139 | 1.072667 | 1.696157 |
| RA_3_6 | -0.4848 | 0.0970 | 1.485463 | 1.090231 | 1.842608 |
| RA_3_7 | -0.4848 | 0.2909 | 1.360126 | 1.047028 | 1.716453 |
| RA_3_8 | -0.4848 | 0.4848 | 1.279424 | 1.000372 | 1.62409 |
| RA_3_9 | -0.4848 | 0.6788 | 1.342337 | 1.06368 | 1.712683 |
| RA_3_10 | -0.4848 | 0.8727 | 1.209707 | 0.966626 | 1.548469 |
| RA_4_1 | -0.2909 | -0.8727 | 1.356277 | 0.981062 | 1.673908 |
| RA_4_2 | -0.2909 | -0.6788 | 1.463013 | 1.038819 | 1.794311 |
| RA_4_3 | -0.2909 | -0.4848 | 1.376534 | 1.035043 | 1.722255 |
| RA_4_4 | -0.2909 | -0.2909 | 1.423225 | 0.994297 | 1.736144 |
| RA_4_5 | -0.2909 | -0.0970 | 1.378511 | 1.06495 | 1.741956 |
| RA_4_6 | -0.2909 | 0.0970 | 1.575282 | 1.057957 | 1.897574 |
| RA_4_7 | -0.2909 | 0.2909 | 1.450006 | 0.989338 | 1.755365 |

Continued on next page

**Table 14 – continued from previous page**

| Sim Name | Description | | X-Error | Y-Error | Total Error |
|---|---|---|---|---|---|
| RA_4_8 | -0.2909 | 0.4848 | 1.432396 | 1.03068 | 1.76467 |
| RA_4_9 | -0.2909 | 0.6788 | 1.430809 | 1.006312 | 1.749251 |
| RA_4_10 | -0.2909 | 0.8727 | 1.346344 | 0.925849 | 1.633965 |
| RA_5_1 | -0.0970 | -0.8727 | 1.675698 | 1.098948 | 2.003908 |
| RA_5_2 | -0.0970 | -0.6788 | 1.759741 | 1.269535 | 2.169887 |
| RA_5_3 | -0.0970 | -0.4848 | 1.746825 | 1.082941 | 2.055276 |
| RA_5_4 | -0.0970 | -0.2909 | 1.740847 | 1.181663 | 2.104014 |
| RA_5_5 | -0.0970 | -0.0970 | 1.819456 | 1.238954 | 2.201233 |
| RA_5_6 | -0.0970 | 0.0970 | 1.895844 | 1.233318 | 2.261703 |
| RA_5_7 | -0.0970 | 0.2909 | 1.769311 | 1.150609 | 2.110536 |
| RA_5_8 | -0.0970 | 0.4848 | 1.753172 | 1.220099 | 2.135943 |
| RA_5_9 | -0.0970 | 0.6788 | 1.7522 | 1.121419 | 2.080333 |
| RA_5_10 | -0.0970 | 0.8727 | 1.604513 | 1.125343 | 1.959811 |
| RA_6_1 | 0.0970 | -0.8727 | 1.017038 | 1.065974 | 1.473318 |
| RA_6_2 | 0.0970 | -0.6788 | 1.137519 | 1.289714 | 1.719684 |
| RA_6_3 | 0.0970 | -0.4848 | 1.048448 | 1.172796 | 1.573116 |
| RA_6_4 | 0.0970 | -0.2909 | 1.030942 | 1.264324 | 1.631366 |
| RA_6_5 | 0.0970 | -0.0970 | 1.124131 | 1.170167 | 1.622641 |

Continued on next page

**Table 14 – continued from previous page**

| Sim Name | Description | | X-Error | Y-Error | Total Error |
|---|---|---|---|---|---|
| RA_6_6 | 0.0970 | 0.0970 | 1.472142 | 1.615431 | 2.185594 |
| RA_6_7 | 0.0970 | 0.2909 | 1.1234 | 1.285113 | 1.70691 |
| RA_6_8 | 0.0970 | 0.4848 | 1.108053 | 1.210595 | 1.641134 |
| RA_6_9 | 0.0970 | 0.6788 | 1.100782 | 1.248883 | 1.664761 |
| RA_6_10 | 0.0970 | 0.8727 | 0.970976 | 1.137779 | 1.495773 |
| RA_7_1 | 0.2909 | -0.8727 | 0.726071 | 1.058925 | 1.28394 |
| RA_7_2 | 0.2909 | -0.6788 | 0.748709 | 1.121757 | 1.348667 |
| RA_7_3 | 0.2909 | -0.4848 | 0.739884 | 1.18308 | 1.395387 |
| RA_7_4 | 0.2909 | -0.2909 | 0.746662 | 1.131368 | 1.355543 |
| RA_7_5 | 0.2909 | -0.0970 | 0.824578 | 1.700247 | 1.889648 |
| RA_7_6 | 0.2909 | 0.0970 | 0.909535 | 1.212543 | 1.515755 |
| RA_7_7 | 0.2909 | 0.2909 | 0.775432 | 1.11772 | 1.360365 |
| RA_7_8 | 0.2909 | 0.4848 | 0.777013 | 1.098114 | 1.345215 |
| RA_7_9 | 0.2909 | 0.6788 | 0.755645 | 1.144768 | 1.371675 |
| RA_7_10 | 0.2909 | 0.8727 | 0.723613 | 1.054346 | 1.278774 |
| RA_8_1 | 0.4848 | -0.8727 | 0.770737 | 1.099183 | 1.342474 |
| RA_8_2 | 0.4848 | -0.6788 | 0.89041 | 1.222947 | 1.512755 |
| RA_8_3 | 0.4848 | -0.4848 | 0.865512 | 1.203668 | 1.482541 |

Continued on next page

**Table 14 – continued from previous page**

| Sim Name | Description | | X-Error | Y-Error | Total Error |
|---|---|---|---|---|---|
| RA_8_4 | 0.4848 | -0.2909 | 0.835812 | 1.156374 | 1.426809 |
| RA_8_5 | 0.4848 | -0.0970 | 0.949901 | 1.392902 | 1.685968 |
| RA_8_6 | 0.4848 | 0.0970 | 0.942929 | 1.185471 | 1.514746 |
| RA_8_7 | 0.4848 | 0.2909 | 0.842919 | 1.156246 | 1.43088 |
| RA_8_8 | 0.4848 | 0.4848 | 0.883446 | 1.146293 | 1.447226 |
| RA_8_9 | 0.4848 | 0.6788 | 0.879595 | 1.185402 | 1.476098 |
| RA_8_10 | 0.4848 | 0.8727 | 0.804812 | 1.113545 | 1.373937 |
| RA_9_1 | 0.6788 | -0.8727 | 0.880253 | 1.065738 | 1.38226 |
| RA_9_2 | 0.6788 | -0.6788 | 0.925849 | 1.140848 | 1.469261 |
| RA_9_3 | 0.6788 | -0.4848 | 0.945219 | 1.165892 | 1.500914 |
| RA_9_4 | 0.6788 | -0.2909 | 0.940107 | 1.150492 | 1.485743 |
| RA_9_5 | 0.6788 | -0.0970 | 1.114677 | 1.475691 | 1.84937 |
| RA_9_6 | 0.6788 | 0.0970 | 1.323962 | 1.579921 | 2.061317 |
| RA_9_7 | 0.6788 | 0.2909 | 0.964876 | 1.152004 | 1.502697 |
| RA_9_8 | 0.6788 | 0.4848 | 0.981249 | 1.171839 | 1.528416 |
| RA_9_9 | 0.6788 | 0.6788 | 0.969685 | 1.178737 | 1.526338 |
| RA_9_10 | 0.6788 | 0.8727 | 0.895281 | 1.086336 | 1.407712 |
| RA_10_1 | 0.8727 | -0.8727 | 0.949568 | 1.062797 | 1.425208 |

Continued on next page

**Table 14 – continued from previous page**

| Sim Name | Description | | X-Error | Y-Error | Total Error |
|---|---|---|---|---|---|
| RA_10_2 | 0.8727 | -0.6788 | 0.997527 | 1.140849 | 1.515453 |
| RA_10_3 | 0.8727 | -0.4848 | 0.978403 | 1.109295 | 1.479124 |
| RA_10_4 | 0.8727 | -0.2909 | 0.988242 | 1.137478 | 1.506811 |
| RA_10_5 | 0.8727 | -0.0970 | 1.064174 | 1.261094 | 1.650099 |
| RA_10_6 | 0.8727 | 0.0970 | 1.111913 | 1.204931 | 1.639576 |
| RA_10_7 | 0.8727 | 0.2909 | 0.999269 | 1.130357 | 1.508724 |
| RA_10_8 | 0.8727 | 0.4848 | 1.004764 | 1.138158 | 1.518207 |
| RA_10_9 | 0.8727 | 0.6788 | 1.024725 | 1.167323 | 1.553288 |
| RA_10_10 | 0.8727 | 0.8727 | 0.942148 | 1.06772 | 1.423963 |

Table 15: Altitude Tests, Full Results

| Sim Name | Description | | X-Error | Y-Error | Total Error |
|---|---|---|---|---|---|
| Baseline | Alt1=3000, Alt2=500 | | 0.936 | 1.193 | 1.516359 |
| Alt_1_1 | 100 | 50 | 1.109583 | 1.364651 | 1.75882 |
| Alt_1_2 | 100 | 377.7778 | 1.110187 | 1.325499 | 1.729006 |
| Alt_1_3 | 100 | 705.5556 | 1.11891 | 1.310728 | 1.723359 |
| Alt_1_4 | 100 | 1033.333 | 1.069261 | 1.273438 | 1.662817 |

Continued on next page

**Table 15 – continued from previous page**

| Sim Name | Description | | X-Error | Y-Error | Total Error |
|---|---|---|---|---|---|
| Alt_1_5 | 100 | 1361.111 | 1.11317 | 1.3539 | 1.752767 |
| Alt_1_6 | 100 | 1688.889 | 1.14289 | 1.361465 | 1.777578 |
| Alt_1_7 | 100 | 2016.667 | 1.145673 | 1.350372 | 1.770896 |
| Alt_1_8 | 100 | 2344.444 | 1.098898 | 1.311365 | 1.710922 |
| Alt_1_9 | 100 | 2672.222 | 1.114867 | 1.305272 | 1.716585 |
| Alt_1_10 | 100 | 3000 | 1.096438 | 1.327171 | 1.7215 |
| Alt_2_1 | 1200 | 50 | 1.139507 | 1.350764 | 1.767212 |
| Alt_2_2 | 1200 | 377.7778 | 1.134436 | 1.34842 | 1.762152 |
| Alt_2_3 | 1200 | 705.5556 | 1.157104 | 1.389556 | 1.808246 |
| Alt_2_4 | 1200 | 1033.333 | 1.059709 | 1.274906 | 1.65782 |
| Alt_2_5 | 1200 | 1361.111 | 1.12037 | 1.344916 | 1.750436 |
| Alt_2_6 | 1200 | 1688.889 | 1.080631 | 1.31315 | 1.700626 |
| Alt_2_7 | 1200 | 2016.667 | 1.111744 | 1.316411 | 1.723053 |
| Alt_2_8 | 1200 | 2344.444 | 1.191835 | 1.382195 | 1.825084 |
| Alt_2_9 | 1200 | 2672.222 | 1.116799 | 1.336343 | 1.741566 |
| Alt_2_10 | 1200 | 3000 | 1.111601 | 1.351795 | 1.750145 |
| Alt_3_1 | 2300 | 50 | 1.132585 | 1.347435 | 1.760207 |
| Alt_3_2 | 2300 | 377.7778 | 1.14772 | 1.338064 | 1.76286 |

Continued on next page

**Table 15 – continued from previous page**

| Sim Name | Description | | X-Error | Y-Error | Total Error |
|---|---|---|---|---|---|
| Alt_3_3 | 2300 | 705.5556 | 1.103434 | 1.318213 | 1.719085 |
| Alt_3_4 | 2300 | 1033.333 | 1.101894 | 1.308431 | 1.710603 |
| Alt_3_5 | 2300 | 1361.111 | 1.08722 | 1.300802 | 1.695327 |
| Alt_3_6 | 2300 | 1688.889 | 1.116673 | 1.343642 | 1.747093 |
| Alt_3_7 | 2300 | 2016.667 | 1.068207 | 1.303376 | 1.685187 |
| Alt_3_8 | 2300 | 2344.444 | 1.128212 | 1.342128 | 1.753331 |
| Alt_3_9 | 2300 | 2672.222 | 1.129495 | 1.351761 | 1.761538 |
| Alt_3_10 | 2300 | 3000 | 1.12642 | 1.353739 | 1.761088 |
| Alt_4_1 | 3400 | 50 | 1.135966 | 1.352575 | 1.766318 |
| Alt_4_2 | 3400 | 377.7778 | 1.135382 | 1.33464 | 1.752243 |
| Alt_4_3 | 3400 | 705.5556 | 1.150352 | 1.358889 | 1.780419 |
| Alt_4_4 | 3400 | 1033.333 | 1.135391 | 1.373326 | 1.781891 |
| Alt_4_5 | 3400 | 1361.111 | 1.134508 | 1.349644 | 1.763136 |
| Alt_4_6 | 3400 | 1688.889 | 1.082446 | 1.273507 | 1.671379 |
| Alt_4_7 | 3400 | 2016.667 | 1.104717 | 1.33171 | 1.730275 |
| Alt_4_8 | 3400 | 2344.444 | 1.139442 | 1.373037 | 1.784253 |
| Alt_4_9 | 3400 | 2672.222 | 1.147308 | 1.346129 | 1.768722 |
| Alt_4_10 | 3400 | 3000 | 1.098282 | 1.288133 | 1.692781 |

Continued on next page

**Table 15 – continued from previous page**

| Sim Name | Description | | X-Error | Y-Error | Total Error |
|---|---|---|---|---|---|
| Alt_5_1 | 4500 | 50 | 1.154532 | 1.384129 | 1.802431 |
| Alt_5_2 | 4500 | 377.7778 | 1.192517 | 1.39553 | 1.835647 |
| Alt_5_3 | 4500 | 705.5556 | 1.14656 | 1.341779 | 1.764928 |
| Alt_5_4 | 4500 | 1033.333 | 1.137146 | 1.341512 | 1.758623 |
| Alt_5_5 | 4500 | 1361.111 | 1.186305 | 1.398047 | 1.833536 |
| Alt_5_6 | 4500 | 1688.889 | 1.158048 | 1.392381 | 1.811022 |
| Alt_5_7 | 4500 | 2016.667 | 1.170804 | 1.375286 | 1.806154 |
| Alt_5_8 | 4500 | 2344.444 | 1.120314 | 1.329549 | 1.738621 |
| Alt_5_9 | 4500 | 2672.222 | 1.152052 | 1.3713 | 1.791002 |
| Alt_5_10 | 4500 | 3000 | 1.137771 | 1.344011 | 1.760934 |
| Alt_6_1 | 5600 | 50 | 1.182617 | 1.372618 | 1.811812 |
| Alt_6_2 | 5600 | 377.7778 | 1.189953 | 1.384418 | 1.825541 |
| Alt_6_3 | 5600 | 705.5556 | 1.160408 | 1.355091 | 1.784045 |
| Alt_6_4 | 5600 | 1033.333 | 1.196105 | 1.406556 | 1.846366 |
| Alt_6_5 | 5600 | 1361.111 | 1.15415 | 1.350313 | 1.776346 |
| Alt_6_6 | 5600 | 1688.889 | 1.18218 | 1.372549 | 1.811475 |
| Alt_6_7 | 5600 | 2016.667 | 1.165635 | 1.355061 | 1.787427 |
| Alt_6_8 | 5600 | 2344.444 | 1.129711 | 1.356089 | 1.764999 |

Continued on next page

**Table 15 – continued from previous page**

| Sim Name | Description | | X-Error | Y-Error | Total Error |
|---|---|---|---|---|---|
| Alt_6_9 | 5600 | 2672.222 | 1.156659 | 1.361137 | 1.786212 |
| Alt_6_10 | 5600 | 3000 | 1.13703 | 1.33903 | 1.756655 |
| Alt_7_1 | 6700 | 50 | 1.190047 | 1.368494 | 1.813556 |
| Alt_7_2 | 6700 | 377.7778 | 1.205536 | 1.426755 | 1.867872 |
| Alt_7_3 | 6700 | 705.5556 | 1.188258 | 1.417801 | 1.849897 |
| Alt_7_4 | 6700 | 1033.333 | 1.172022 | 1.389674 | 1.817919 |
| Alt_7_5 | 6700 | 1361.111 | 1.179956 | 1.362237 | 1.802217 |
| Alt_7_6 | 6700 | 1688.889 | 1.182466 | 1.387766 | 1.823217 |
| Alt_7_7 | 6700 | 2016.667 | 1.1736 | 1.370973 | 1.80469 |
| Alt_7_8 | 6700 | 2344.444 | 1.154448 | 1.377884 | 1.797586 |
| Alt_7_9 | 6700 | 2672.222 | 1.164425 | 1.376251 | 1.802763 |
| Alt_7_10 | 6700 | 3000 | 1.134433 | 1.316459 | 1.737815 |
| Alt_8_1 | 7800 | 50 | 1.226228 | 1.420823 | 1.876799 |
| Alt_8_2 | 7800 | 377.7778 | 1.275706 | 1.47576 | 1.950716 |
| Alt_8_3 | 7800 | 705.5556 | 1.234521 | 1.422036 | 1.883143 |
| Alt_8_4 | 7800 | 1033.333 | 1.19011 | 1.381435 | 1.823383 |
| Alt_8_5 | 7800 | 1361.111 | 1.219531 | 1.430131 | 1.879503 |
| Alt_8_6 | 7800 | 1688.889 | 1.176894 | 1.401351 | 1.82999 |

Continued on next page

**Table 15 – continued from previous page**

| Sim Name | Description | | X-Error | Y-Error | Total Error |
|---|---|---|---|---|---|
| Alt_8_7 | 7800 | 2016.667 | 1.225417 | 1.436894 | 1.888468 |
| Alt_8_8 | 7800 | 2344.444 | 1.222505 | 1.443211 | 1.891396 |
| Alt_8_9 | 7800 | 2672.222 | 1.181915 | 1.376322 | 1.814163 |
| Alt_8_10 | 7800 | 3000 | 1.172717 | 1.382035 | 1.812536 |
| Alt_9_1 | 8900 | 50 | 1.342625 | 1.54456 | 2.046535 |
| Alt_9_2 | 7800 | 377.7778 | 1.271102 | 1.463837 | 1.93869 |
| Alt_9_3 | 7800 | 705.5556 | 1.261296 | 1.46143 | 1.930452 |
| Alt_9_4 | 7800 | 1033.333 | 1.276652 | 1.492805 | 1.964258 |
| Alt_9_5 | 7800 | 1361.111 | 1.206788 | 1.411403 | 1.856986 |
| Alt_9_6 | 7800 | 1688.889 | 1.233397 | 1.427886 | 1.88683 |
| Alt_9_7 | 7800 | 2016.667 | 1.232969 | 1.439231 | 1.895152 |
| Alt_9_8 | 7800 | 2344.444 | 1.20748 | 1.375171 | 1.830055 |
| Alt_9_9 | 7800 | 2672.222 | 1.202118 | 1.402643 | 1.847294 |
| Alt_9_10 | 7800 | 3000 | 1.175048 | 1.377338 | 1.810469 |
| Alt_10_1 | 10000 | 50 | 1.374715 | 1.569243 | 2.086233 |
| Alt_10_2 | 10000 | 377.7778 | 1.288248 | 1.469931 | 1.954554 |
| Alt_10_3 | 10000 | 705.5556 | 1.276719 | 1.458635 | 1.93846 |
| Alt_10_4 | 10000 | 1033.333 | 1.30683 | 1.477073 | 1.972194 |

Continued on next page

**Table 15 – continued from previous page**

| Sim Name | Description | | X-Error | Y-Error | Total Error |
|---|---|---|---|---|---|
| Alt_10_5 | 10000 | 1361.111 | 1.276039 | 1.456364 | 1.936304 |
| Alt_10_6 | 10000 | 1688.889 | 1.237957 | 1.396908 | 1.866518 |
| Alt_10_7 | 10000 | 2016.667 | 1.218708 | 1.420567 | 1.8717 |
| Alt_10_8 | 10000 | 2344.444 | 1.25564 | 1.434935 | 1.906743 |
| Alt_10_9 | 10000 | 2672.222 | 1.235964 | 1.414512 | 1.878417 |
| Alt_10_10 | 10000 | 3000 | 1.233478 | 1.441371 | 1.897108 |

Table 16: Separation Distance Tests, Full Results

| Sim Name | Description | X-Error | Y-Error | Total Error |
|---|---|---|---|---|
| Baseline | D=10,000 | 0.936 | 1.193 | 1.516359 |
| Dist_1 | 500 | 0.972052 | 1.242916 | 1.577886 |
| Dist_2 | 5736.842 | 0.962577 | 1.221914 | 1.555515 |
| Dist_3 | 10973.68 | 0.979452 | 1.244575 | 1.58376 |
| Dist_4 | 16210.53 | 0.964501 | 1.221851 | 1.556658 |
| Dist_5 | 21447.37 | 0.972691 | 1.257889 | 1.590098 |
| Dist_6 | 26684.21 | 0.985487 | 1.271303 | 1.608538 |
| Dist_7 | 31921.05 | 0.974231 | 1.259472 | 1.592293 |

Continued on next page

**Table 16 – continued from previous page**

| Sim Name | Description | X-Error | Y-Error | Total Error |
|---|---|---|---|---|
| Dist_8 | 37157.89 | 0.965385 | 1.196369 | 1.537292 |
| Dist_9 | 42394.74 | 0.920412 | 1.171081 | 1.489493 |
| Dist_10 | 47631.58 | 1.001211 | 1.204616 | 1.566372 |
| Dist_11 | 52868.42 | 0.936262 | 1.168227 | 1.497111 |
| Dist_12 | 58105.26 | 0.991917 | 1.251233 | 1.596711 |
| Dist_13 | 63342.11 | 0.992052 | 1.232606 | 1.582241 |
| Dist_14 | 68578.95 | 0.983957 | 1.262575 | 1.600709 |
| Dist_15 | 73815.79 | 0.974755 | 1.25192 | 1.586648 |
| Dist_16 | 79052.63 | 0.996322 | 1.218286 | 1.57381 |
| Dist_17 | 84289.47 | 0.942571 | 1.219915 | 1.541634 |
| Dist_18 | 89526.32 | 0.947248 | 1.253686 | 1.571308 |
| Dist_19 | 94763.16 | 0.993933 | 1.240476 | 1.589555 |
| Dist_20 | 100000 | 0.951802 | 1.195667 | 1.528249 |

Table 17: Range Sensor Noise Tests, Full Results

| Sim Name | Description | X-Error | Y-Error | Total Error |
|---|---|---|---|---|
| Baseline | R=0.1 | 0.936 | 1.193 | 1.516359 |

Continued on next page

**Table 17 – continued from previous page**

| Sim Name | Description | X-Error | Y-Error | Total Error |
|---|---|---|---|---|
| Rval_1 | 1.00E-03 | 0.371148 | 0.410636 | 0.55351 |
| Rval_2 | 0.4588325 | 1.45857 | 1.63741 | 2.192838 |
| Rval_3 | 0.648886374 | 1.550201 | 1.750322 | 2.338108 |
| Rval_4 | 0.794719944 | 1.669034 | 1.851475 | 2.492716 |
| Rval_5 | 0.917663366 | 1.723605 | 1.916918 | 2.577865 |
| Rval_6 | 1.025978711 | 1.760053 | 2.039337 | 2.693823 |
| Rval_7 | 1.123903278 | 1.797572 | 2.036852 | 2.716622 |
| Rval_8 | 1.213954217 | 1.822074 | 2.056832 | 2.747819 |
| Rval_9 | 1.297771592 | 1.888238 | 2.110371 | 2.831803 |
| Rval_10 | 1.376494594 | 1.890867 | 2.139127 | 2.855038 |
| Rval_11 | 1.450952663 | 1.917537 | 2.197462 | 2.916468 |
| Rval_12 | 1.521771959 | 1.923888 | 2.176171 | 2.904663 |
| Rval_13 | 1.589438944 | 1.943988 | 2.21318 | 2.945718 |
| Rval_14 | 1.654340479 | 1.972673 | 2.2301 | 2.977379 |
| Rval_15 | 1.716790227 | 2.007757 | 2.247941 | 3.014021 |
| Rval_16 | 1.777046693 | 1.992074 | 2.288872 | 3.034352 |
| Rval_17 | 1.835325914 | 2.021212 | 2.297025 | 3.059677 |
| Rval_18 | 1.891810634 | 2.032827 | 2.303035 | 3.071866 |

Continued on next page

**Table 17 – continued from previous page**

| Sim Name | Description | X-Error | Y-Error | Total Error |
|---|---|---|---|---|
| Rval_19 | 1.946657067 | 2.087049 | 2.36814 | 3.156558 |
| Rval_20 | 2 | 2.08639 | 2.339812 | 3.134923 |

Table 18: Daughter-Ship IMU Uncertainty Tests, Full Results

| Sim Name | Description | X-Error | Y-Error | Total Error |
|---|---|---|---|---|
| Baseline | $Q=0.01^2$ | 0.936 | 1.193 | 1.516359 |
| Qval_1 | 1.00E-05 | 0.169246 | 0.181702 | 0.248314 |
| Qval_2 | 5.74E-03 | 0.834511 | 0.930255 | 1.249714 |
| Qval_3 | 0.008111077 | 0.923565 | 1.037458 | 1.388989 |
| Qval_4 | 0.009933997 | 0.97189 | 1.108861 | 1.474497 |
| Qval_5 | 0.01147079 | 1.01951 | 1.159786 | 1.544184 |
| Qval_6 | 0.012824732 | 1.043392 | 1.172271 | 1.569359 |
| Qval_7 | 0.01404879 | 1.067231 | 1.219672 | 1.620674 |
| Qval_8 | 0.015174427 | 1.105635 | 1.233031 | 1.656139 |
| Qval_9 | 0.016222144 | 1.136525 | 1.252068 | 1.690966 |
| Qval_10 | 0.017206182 | 1.155599 | 1.300628 | 1.73984 |
| Qval_11 | 0.018136908 | 1.177497 | 1.311137 | 1.762265 |

Continued on next page

**Table 18 – continued from previous page**

| Sim Name | Description | X-Error | Y-Error | Total Error |
|---|---|---|---|---|
| Qval_12 | 0.019022149 | 1.202118 | 1.338987 | 1.799437 |
| Qval_13 | 0.019867986 | 1.211898 | 1.350845 | 1.814794 |
| Qval_14 | 0.020679256 | 1.231218 | 1.39376 | 1.859694 |
| Qval_15 | 0.021459877 | 1.224467 | 1.39452 | 1.855804 |
| Qval_16 | 0.022213083 | 1.260763 | 1.405996 | 1.888478 |
| Qval_17 | 0.022941574 | 1.296518 | 1.447713 | 1.943407 |
| Qval_18 | 0.023647633 | 1.286772 | 1.440437 | 1.931487 |
| Qval_19 | 0.024333213 | 1.298724 | 1.488027 | 1.975072 |
| Qval_20 | 0.025 | 1.337063 | 1.509094 | 2.016209 |

# Bibliography


1. Thomas P Ehrhard. Air Force UAVs: The Secret History. *The Mitchell Institute for Airpower Studies*, (July):89, 2010.

2. Thomas Wildenberg. Origins of Inertial Navigation. 63(4):17–24, 2016.

3. David Titterton, John L Weston, and John Weston. *Strapdown inertial navigation technology*, volume 17. IET, 2004.

4. Zupt's inertial technology systems information. `https://www.zupt.com/inertial-technology/`, Sep 2015. Accessed: 2020-12-07.

5. John Raquet. EENG 533 Navigation Using the GPS Course Slides, 2020.

6. Gps.gov: Control segment. `https://www.gps.gov/systems/gps/control/`. Accessed: 2020-12-08.

7. Error analysis for the global positioning system. `https://en.wikipedia.org/wiki/Error_analysis_for_the_Global_Positioning_System`. Accessed: 2021-01-12.

8. R. T. Ioannides, T. Pany, and G. Gibbons. Known vulnerabilities of global navigation satellite systems, status, and potential mitigation techniques. *Proceedings of the IEEE*, 104(6):1174–1194, 2016.

9. Peter S Maybeck. *Stochastic models, estimation, and control*. Academic press, 1982.

10. Aaron Canciani. EENG 765 Stochastic Estimation and Control I Course Slides, 2019.

11. Aaron Canciani. EENG 766 Stochastic Estimation and Control II Course Slides, 2020.

12. Robert Grover Brown and Patrick YC Hwang. Introduction to random signals and applied kalman filtering: with matlab exercises and solutions. *itrs*, 1997.

13. Liang Boon Wee, Wei Sheng, Eugene Lee, and Haoyong Yu. A Unified Method for Vision Aided Navigation of Autonomous Systems. *2020 IEEE/ION Position, Location and Navigation Symposium, PLANS 2020*, pages 1635–1641, 2020.

14. R. Madison, G. Andrews, P. Debitetto, S. Rasmussen, and M. Bottkol. Vision-aided navigation for small UAVs in GPS-challenged environments. *Collection of Technical Papers - 2007 AIAA InfoTech at Aerospace Conference*, 3(September 2015):2733–2745, 2007.

15. Lvtianyang Zhang, Mengbin Ye, Brian D.O. Anderson, Peter Sarunic, and Hatem Hmam. Cooperative localisation of UAVs in a GPS-denied environment using bearing measurements. In *2016 IEEE 55th Conference on Decision and Control, CDC 2016*, pages 4320–4326, 2016.

16. Rajnikant Sharma and Clark Taylor. Cooperative navigation of MAVs in GPS denied areas. *IEEE International Conference on Multisensor Fusion and Integration for Intelligent Systems*, (4):481–486, 2008.

17. Aaron J. Canciani and Christopher J. Brennan. An Analysis of the Benefits and Difficulties of Aerial Magnetic Vector Navigation. *IEEE Transactions on Aerospace and Electronic Systems*, 56(6):1–1, 2020.

18. Jeremy Hardy, Jared Strader, Jason N. Gross, Yu Gu, Mark Keck, Joel Douglas, and Clark N. Taylor. Unmanned aerial vehicle relative navigation in GPS denied

environments. *Proceedings of the IEEE/ION Position, Location and Navigation Symposium, PLANS 2016*, pages 344–352, 2016.

19. Jared Strader, Yu Gu, Jason N. Gross, Matteo De Petrillo, and Jeremy Hardy. Cooperative relative localization for moving UAVs with single link range measurements. *Proceedings of the IEEE/ION Position, Location and Navigation Symposium, PLANS 2016*, pages 336–343, 2016.

20. Derek R. Nelson, D. Blake Barber, Timothy W. McLain, and Randal W. Beard. Vector field path following for miniature air vehicles. *IEEE Transactions on Robotics*, 23(3):519–529, 2007.

21. Ac-130u, u.s. air force, fact sheet display. `https://www.af.mil/About-Us/Fact-Sheets/Display/Article/104486/ac-130u/`, Jan 2016. Accessed: 2021-01-05.

22. Area-I. ALTIUS-600 Fact Sheet. `https://areai.com/altius-600-2/`. Accessed: 2021-01-05.

23. Root-mean-square deviation. `https://en.wikipedia.org/wiki/Root-mean-square_deviation`. Accessed: 2021-01-08.

# Acronyms

**AWGN** Additive White Gaussian Noise. 11

**C/A** coarse-acquisition. 9

**DoD** Department of Defense. iv, 1

**EKF** Extended Kalman Filter. iv, 13

**GNSS** Global Navigation Satellite System. 7

**GPS** Global Positioning System. iv, 1

**IMU** inertial measurement unit. iv

**ISR** Intelligence, Surveillance, and Reconnaissance. 1

**MAVs** Miniature Air Vehicles. 16

**NRO** National Reconnaissance Office. 4

**P** precise. 9

**PRN** Pseudo-Random Noise. 9

**RF** Radio Frequency. 9

**RMS error** root-mean-square error. 29

**SPIRE** Space Inertial Reference Equipment. 6

**UAVs** Unmanned Aerial Vehicles. iv, 1

**USAF** United States Air Force. 4

# REPORT DOCUMENTATION PAGE

*Form Approved*
*OMB No. 0704–0188*



| 1. REPORT DATE *(DD–MM–YYYY)* | 2. REPORT TYPE | 3. DATES COVERED *(From — To)* |
|---|---|---|
| 25–03–2021 | Master's Thesis | Sept 2019 — Mar 2021 |

**4. TITLE AND SUBTITLE**

GPS-Denied Localization of Daughter-Ships in a Mother-Daughter Ship Collaborative Environment

**5a. CONTRACT NUMBER**

**5b. GRANT NUMBER**

**5c. PROGRAM ELEMENT NUMBER**

**6. AUTHOR(S)**

Jacquin, Ethan W, Capt

**5d. PROJECT NUMBER**

**5e. TASK NUMBER**

**5f. WORK UNIT NUMBER**

**7. PERFORMING ORGANIZATION NAME(S) AND ADDRESS(ES)**

Air Force Institute of Technology
Graduate School of Engineering and Management (AFIT/EN)
2950 Hobson Way
WPAFB OH 45433-7765

**8. PERFORMING ORGANIZATION REPORT NUMBER**

AFIT-ENG-MS-21-M-051

**9. SPONSORING / MONITORING AGENCY NAME(S) AND ADDRESS(ES)**

AFRL/RQQC
Building 146
WPAFB OH 45433-7765
DSN 798-4628, COMM 937-938-4628
Email: paul.fleitz@us.af.mil

**10. SPONSOR/MONITOR'S ACRONYM(S)**

AFRL/RQQC

**11. SPONSOR/MONITOR'S REPORT NUMBER(S)**

**12. DISTRIBUTION / AVAILABILITY STATEMENT**

DISTRIBUTION STATEMENT A:
APPROVED FOR PUBLIC RELEASE; DISTRIBUTION UNLIMITED.

**13. SUPPLEMENTARY NOTES**

**14. ABSTRACT**

This research investigates the possibility of using the communication link between a mothership and daughter-ship UAV and an Extended Kalman Filter algorithm as a replacement of GPS, assuming a ranging link exists between the mothership and daughter-ship and that the mothership is GPS-enabled. A simulation study examines the viability of the approach and the effect of parameters such as distance, altitude, roll angle, speed, ranging sensor noise, and inertial measurement unit uncertainty were considered. The magnitude of the errors between predicted and measured position were examined and a range of acceptable flight parameters was formed.

**15. SUBJECT TERMS**

GPS-Denied Navigation, Inertial Navigation System, Unmanned Aerial Vehicle, Extended Kalman Filter

| 16. SECURITY CLASSIFICATION OF: | | | 17. LIMITATION OF ABSTRACT | 18. NUMBER OF PAGES | 19a. NAME OF RESPONSIBLE PERSON |
|---|---|---|---|---|---|
| a. REPORT | b. ABSTRACT | c. THIS PAGE | | | Captain Ethan W. Jacquin, AFIT/ENG |
| U | U | U | UU | 97 | 19b. TELEPHONE NUMBER *(include area code)* (937) 255-3636; ethan.jacquin@afit.edu |